A DENSITY FUNCTIONAL THEORY STUDY OF DUAL SURFACTANT EFFECT IN ENHANCING P-TYPE DOPING IN III-V SEMICONDUCTORS

by

Junyi Zhu

A dissertation submitted to the faculty of
The University of Utah
in partial fulfillment of the requirements for the degree of

Doctor of Philosophy

Department of Materials Science and Engineering

The University of Utah

May 2010

UMI Number: 3405690

All rights reserved

INFORMATION TO ALL USERS
The quality of this reproduction is dependent upon the quality of the copy submitted.

In the unlikely event that the author did not send a complete manuscript
and there are missing pages, these will be noted. Also, if material had to be removed,
a note will indicate the deletion.

UMI 3405690
Copyright 2010 by ProQuest LLC.
All rights reserved. This edition of the work is protected against
unauthorized copying under Title 17, United States Code.

ProQuest LLC
789 East Eisenhower Parkway
P.O. Box 1346
Ann Arbor, MI 48106-1346

Copyright © Junyi Zhu 2010

All Rights Reserved

THE UNIVERSITY OF UTAH GRADUATE SCHOOL

SUPERVISORY COMMITTEE APPROVAL

of a dissertation submitted by

Junyi Zhu

This dissertation has been read by each member of the following supervisory committee and by majority vote has been found to be satisfactory.

Date	Signature
9/8/09	Chair: Feng Liu
9/8/09	Gerald B. Stringfellow
9-8-09	Anil Virkar
9/8/09	Clayton Williams
9/8/09	Mark Miller

THE UNIVERSITY OF UTAH GRADUATE SCHOOL

FINAL READING APPROVAL

To the Graduate Council of the University of Utah:

I have read the dissertation of Junyi Zhu in its final form and have found that (1) its format, citations, and bibliographic style are consistent and acceptable; (2) its illustrative materials including figures, tables, and charts are in place; and (3) the final manuscript is satisfactory to the supervisory committee and is ready for submission to The Graduate School.

9/8/09
Date

Feng Liu
Chair: Supervisory Committee

Approved for the Major Department

Anil Virkar
Chair/Dean

Approved for the Graduate Council

Charles A. Wight
Dean of The Graduate School

ABSTRACT

Surfactant effects are usually achieved by the addition of a single surface element. We demonstrate by density functional theory calculations a dual-surfactant effect of Sb and H on enhancing Zn, Mg, Be and Cd incorporation in OMVPE grown GaP thin films. The combined effects of Sb and H lower significantly the film doping energy during the epitaxial growth of all the *p*-type dopants studied, while neither Sb nor H canh work alone as effectively. The role of H is to satisfy the electron counting rule. The role of Sb is to serve as an electron reservoir to help electron redistribution. We also predict that due to the low electronegativity of Mg, Sb and H will enhance Mg doping the least among these dopants because Mg as an electron reservoir itself may negate the electron reservoir effect of Sb. Our finding suggests a general strategy for enhancing p-type doping of III-V semiconductors by using a metallic-element with H as dual-surfactants and provides an important general physical understanding for *p*-type doping in III-V thin films.

We also discovered an intriguing dopant induced electronic stress effect. First principles calculation reveals that even if a dopant has the same atomic size as the host atom it substitutes, it still induces a lattice stress of electronic origin, because it has either one more or one less electron than the host. In general, an n-type dopant induces a compressive electronic stress, and a p-type dopant induces a tensile stress. We also found that the electronic stress exhibits a nonlinear dependence on strain, different from the conventional atomic stress effect. The discovery of electronic stress has significant

implications in using external strain to enhance doping. In general, the competition between the atomic stress and electronic stress determines the overall stress induced by a dopant, which in turn determines how external strain will change the doping energy.

TABLE OF CONTENTS

ABSTRACT iv

LIST OF FIGURES...viii

ACKNOWLEDGEMENTS x

CHAPTER page

1. INTRODUCTION..1

1.1 Doping, codoping and p-type doping in wide gap semiconductors................1
1.2 Surfactant enhanced doping in GaP/InGaP..8
1.3 Review of surfactant effects..11
1.4 Electron counting model...18
1.5 References...24

2. METHODOLOGY..27

2.1 Review of Density-Functional-Theory..27
2.2 The Kohn-Sham ansatz...29
2.3 Solving the Kohn-Sham equations..32
2.4 Pseudopotential...34
2.5 Supercell technique and simulation set-up..37
2.6 References...39

3. DUAL-SURFACTANT EFFECT OF SB AND
H ON ENHANCING ZN DOPING IN GAP...41

3.1 References...53

4. DUAL-SURFACTANT EFFECT OF SB AND H ON ENHANCING
CATION-SUBSTITUTED P-TYPE DOPING IN GAP.......................................55

4.1 References...77

5. DOPANT INDUCED ELECTRONIC STRESS
AND STRAIN ENHANCED DOPING...80

5.1 The dopant induced electronic stress in semiconductors...............................81

5.2 The effect of strain on doping energy....87
5.3 The nonlinear strain dependence of electronic stress....91
5.4 Enhanced doping using Epitaxial Strain....95
5.5 References....97

6. CONCLUSION....99

LIST OF FIGURES

Figure page

1.1 Band offsets and the Fermi level stabilization energy in III-V compounds..........5

1.2 Schematic illustration of In and 2 N, codoped into ZnSe..............................7

1.3 SIMS depth profile of Zn-doped GaInP..10

1.4 Ion backscattering spectra for Ge/Si(001) films grown at 500 C......................12

1.5 Schematic illustration of different growth modes......................................14

1.6 The missing dimer structure of GaP surface reconstruction...........................19

1.7 Schematic illustration of a 2x2 surface reconstruction for GaP with H adsorbed on top dimers..22

2.1 Calculation of Kohn Sham ground state..33

2.2 Schematic illustration of a pseudo-potential..36

2.3 Schematic illustration of an all electron calculated wave function (solid line), a norm conserving pseudo-potential calculated one (dotted) and an ultra-soft pseudo-potential calculated one(dashed)....................................36

2.4 Schematic illustration of GaP supercell slab..38

3.1 Schematic illustration of various doping configurations, with one Zn atom replacing a Ga atom in the second atomic layer............................44

3.2 Ball-and-stick schematic illustration of one Zn atom doped in the fourth atomic layer (the second cation layer)..44

3.3 Schematic illustration of a plausible doping process, with one Zn atom replacing a Ga atom in GaP film..51

3.4 Change of doping energy at each corresponding step as shown in Fig. 3.3..........51

4.1 Schematic of GaP supercell slab...59

4.2 Schematic illustration of various doping configurations, with one P-type dopant atom replacing a Ga atom in the second atomic layer................61

4.3 Ball-and-stick schematic illustration of one p type dopant atom doped in the fourth atomic layer (the second cation layer)...................................62

4.4 Schematic illustration of a plausible doping process, with one Mg(Zn) atom replacing a Ga atom in GaP film.. 73

4.5 Change of doping energy at each doping step as shown in Fig. 4.4...................74

5.1 Schematic illustration of a dopant induced stress applied to a 2D lattice............82

5.2 Doping energy vs. hydrostatic strain for the dopants studied..........................89

5.3 Dopant induced stress vs. hydrostatic strain...92

5.4 Doping energy of Zn and Si versus hydrostatic strain, showing the excellent fitting of the elastic theory (red solid line) to the DFT calculated data (black dots)...94

5.5 Doping energy vs. biaxial strain and hydrostatic strain for Be in GaP...............96

ACKNOWLEDGEMENTS

I would like to express my sincere gratitude to my advisors, Dr. Feng Liu and Dr Gerald B. Stringfellow, for their inspiration, patient guidance, and insightful instructions during the entire period of this research. Special thanks are also extended to Dr. Anil Virka for his important comments in CHAPTER III and IV. Appreciation is also extended to Zheng Liu for his useful discussions in CHAPTER V. I am grateful to DOE-BES for supporting all the research work. The calculations were performed on AMD Opteron cluster at the CHPC, University of Utah.

Finally, I dedicate this thesis to my beloved wife, Xuan Xiong. Without her never-ending support, this thesis would be impossible to finish.

CHAPTER 1

INTRODUCTION

1.1. Doping, codoping and p-type doping in wide gap semiconductors

Doping has been one of the most important issues in semiconductors. A dopant is a foreign element having a different number of valence electrons from the atom it substitutes. When the dopant is incorporated into an intrinsic semiconductor material, it shifts the Fermi energy of that material, changes the electrical properties and makes the semiconductor extrinsic. There are two types of dopants. One is p-type, which provides one less electron and creates holes as the major carrier. The other is n-type, which provides one more electron as the major carrier. Dopants can be considered as the life blood of semiconductors. Without doping, it is impossible to inject free carriers into semiconductors and most semiconductors would remain intrinsic and insulating at room temperature.

The history of doping can be traced back to the early work of Woodyard during World War II at the Sperry Corporation [1]. Woodyard doped P/As/Sb into Ge and discovered a nonlinear and unidirectional property of Ge [1]. This pioneering work is very important in the history of the semiconductor. Intrinsic semiconductors are often insulators. Only after doping is it possible to design various electronic devices and applications widely used today. Woodyard's work also led to the success of the first Ge-based transistor, invented in 1947 at Bell Labs [2].

In the modern semiconductor industry, doping remains a very important issue. In

the past 20 years, short wavelength (blue or ultraviolet) optoelectronic devices have significantly progressed [3-5]. These devices are usually based on III-nitrides or II-VI wide band gap semiconductors. The nature of most semiconductor devices, such as p-n junctions, tunnel junctions of solar cells, field effect transistors, etc., requires both n- and p- type doping. Achieving a high p-type doping level in many wide band gap materials still remains a challenging problem and overcoming this problem may lead to a new era of technology advances.

Group III-nitrides and group III-phosphides are of special interest because they are widely used in light emitting diodes (LEDs), the major candidates for the replacement of conventional incandescent lamps. These devices can offer long-term reliability, lower power consumptions and lower operating heat. These high efficiency devices are already on the market for high optical power lamps. For example, they are employed in automotive applications and supply interior and exterior lighting. They are also widely used in large screen and projection displays.

Among these nitrides and phosphides, AlGaInP provides the best choice for applications in the range between red and yellow. It is widely used in manufacture of high brightness red, orange and amber LEDs and red diode lasers. However, it is very difficult to make p-type doping in a material. When the band gap becomes larger, it becomes more difficult to dope. Fundamental understanding of AlGaInP is required to improve the electronic and optic properties, especially those properties related to doping. However, AlGaInP is a complex alloy that gives a lot of difficulties and complexity for density functional theory (DFT) studies. This is because to simulate random alloys, a large super cell has to be constructed and a lot of random alloy configurations have to be

calculated to achieve a meaningful average result. Thus, GaP can be a good model system to study the general doping problems. In this thesis, various doping problems of GaP will be extensively studied.

There are three major difficulties in the doping of wide band gap materials, such as nitrides, phosphides and group II-VI semiconductors. One is the limited solubility. Some impurity atoms can not incorporate into the host lattice because the solubility of the dopants is too low. Some dopants may form other different compounds. For example, when N is doped into ZnSe, a compound phase of Zn_3N_2 may occur [6]. Some dopants may lead to segregation or some may substitute the wrong host site to limit a certain type of doping. Another difficulty is that some dopants may form a deep level, so the activation energy of it can be very high and the dopant is not ionized at normal temperatures. Those dopants may form highly localized centers. For example, Mg in GaN can form a localized center with a very high activation energy [7]. The third difficulty is the compensation effect. The dopant may incorporate into the host lattice with another opposite charged defect and form a neutral center. H, Li and Cu are highly mobile impurities. They can passivate dopants in semiconductors [8]. H is especially important in materials grown by Organometallic Vapor-Phase Epitaxy (OMVPE). There exists atomic H near the crystal surface in the growth chamber that may diffuse into the bulk, forming H-dopant-host element complexes that passivate the dopants. Sometimes, those dopants can be activated by thermal annealing. Despite this, in this work, we will demonstrate that H can assist the electron redistribution during the doping processes and play a positive role in the doping, which will be extensively covered in the following chapters. For AlGaInP, GaP, InP and nitrides, it has

long been known that p-type doping is difficult. One phenomenological physical explanation of the difficulty of p-type doping in wide semiconductors was proposed by Walukiewics [8]. He claimed that the maximum doping concentration is an intrinsic property of a given semiconductor, which is determined by the location of the semiconductor band edges with respect to the Fermi level stabilization energy [8]. The Fermi level stabilization energy is defined as when thematerials are heavily damaged by high energy gamma rays or electrons, the Fermienergy stabilizes at a certain energy and becomes insensitive to further damages. This is an intrinsic property of the materials. For III-V semiconductors, the Fermi stabilization energy is about 4.9 eV below the vacuum level [8]. Fig 1.1 shows the band offsets and the Fermi level stabilization energy in III-V compounds [8]. When the Fermi stabilization energy is close to the valence band maximum, the semiconductor is intrinsically p-type, then n-type doping can be difficult to achieve. When the Fermi stabilization energy is close to the conduction band minimum, the semiconductor is intrinsically n-type, then the p-type doping can be difficult to achieve. From Fig 1.1, we observe that the Fermi stabilization energy for GaP is about in the middle of the band gap, which is about 0.9 eV higher than the valence band maximum. However, the Fermi stabilization energy for GaAs is only 0.6 eV above its valence band maximum, so the p-type doping for GaP is relatively difficult compared with GaAs. Also, this theory may explain why it is difficult to dope AlGaInP p-type. Fig 1.1 shows that the Fermi stabilization energy of AlP is about 1.3 eV higher than the valence band maximum. Overall, this theory is successful in explaining the intrinsic difficulties of p-type doping in wide gap materials [8]. However, it is phenomenological and the underlying physical mechanism is still unclear.

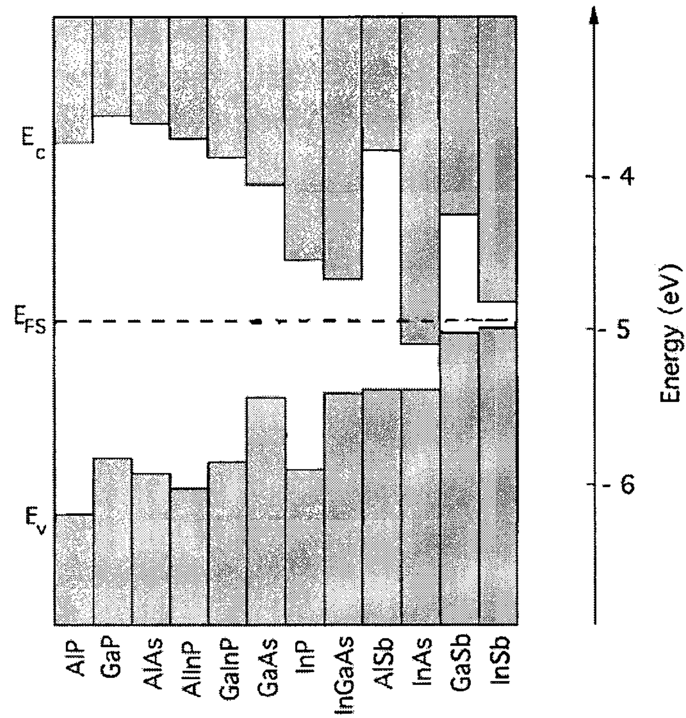

Fig 1.1, Band offsets and the Fermi level stabilization energy in III-V compounds. (Adapted from Reference [8].)

Various ways to improve doping have been proposed in recent years. Codoping and ion implantation are two effective ways to improve the doping in wide band gap materials and they are often implemented together to achieve the maximum doping enhancement.

In Chapman's work [9], the enhancement of the doping of Zn together with H was discovered. So it's worthwhile to examine the concept of codoping. Codoping is to dope p-type and n-type dopants at the same time with the ratio of 2:1 (in some cases, when H is involved, they can be 1:1, and thermal annealing is required to remove the codoped H). There are still debates on whether codoping reduces doping energy or the activation barrier of the dopant [10, 11]. A lot of patents on codoping were filed and Nichia is believed to use codoping to enhance the doping and performance of their blue LED products [12]. In 1997, Yoshida and Yamamoto published the first important work on codoping. They found that codoping improves the acceptor carrier density for GaN and ZnSe [10]. They proposed a possible physical mechanism based on their DFT study. They found that the electrostatic energy (Madelung energy) is increased for p-type dopants, because the 2p orbital of N for GaN or 4p orbital of Se for ZnSe is shifted towards a higher energy region [10]. This leads to a destabilization of ionic charge distributions in both compounds and results in self compensation of anion intrinsic defects [10]. The codoping can decrease the Madelung energy and increase the acceptor carrier density [10]. Fig 1.2 shows a schematic illustration of In and 2 N doped into ZnSe [10]. However, their calculation of 2 Mg/O doped into GaN actually indicated an increase of Madelung energy comparing with 1 Mg case. Zhang et al. [11] found that there is no doping energy gain for codoped 2N and In in ZnSe and they proposed another possible physical mechanism: the codoped dopants are usually doped into the host lattice

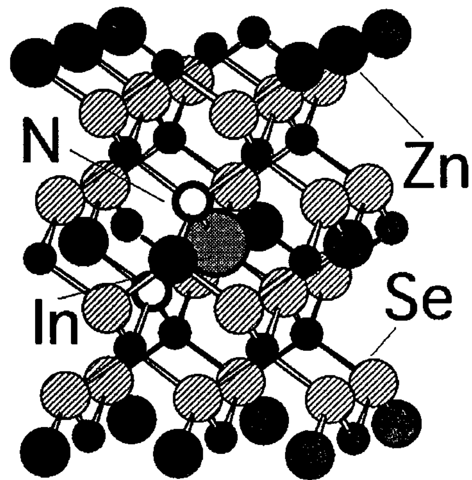

Fig 1.2, Schematic illustration of In and 2 N, codoped into ZnSe. (Adapted from Reference [10].)

as a complex or molecule and they may suppress some other different compound phases and improve doping [11]. Despite the success of codoping in GaN and ZnSe, codoping still brings some concerns. For example, once the p-type and n-type complex are codoped into the lattice, the n-type defects are very difficult to remove and the carrier mobility may decrease because of them.

Ion implantation is also a widely used technique to improve doping in wide band gap materials [12]. With ion beam bombarding the lattice, the dopants can often incorporate in a high concentration and this technique can be applied in both molecular beam epitaxy(MBE) or OMVPE. However, there are also some fundamental problems with this method. One problem is that ion beam may destroy the lattice and create a lot of defects, so that the mobility of the carriers decreases [12]. Therefore, even if the doping level increases, the mobility of the carriers may decrease and the overall performance can be affected. Also, ion beam may not enhance the activation barrier of the dopant, so even if the doping concentration increases, the carrier concentration may not improve [12]. For LEDs, ion beam implantation is never used because of the large amount of defects it creates.

1.2. Surfactant enhanced doping in GaP/InGaP

One of the recent improvements of doping in wide band gap materials involves the use of surfactants. Sb and Bi are good surfactants for GaP/InGaP systems because of their low incorporation and low volatility [9]. Surfactant enhanced doping was first studied in the GaAs system [13]. However, the concentrations of Te and P were not affected during OMVPE growth of GaAs [13]. Later, Sb was found to enhance the doping of Zn in GaAS [13]. This effect was attributed to the improvement of surface diffusion. Chapman et al.

found that when Sb as surfactant is incorporated into GaP/InGaP, the concentration of Zn is improved by more than an order of magnitude [9]. Fig 1.3 shows the SIMS profile from their experiment [9]. The dashed curve shows the concentration of Zn. In the region where Sb is added, the concentration of Zn is improved by an order of magnitude as compared with the case without Sb. The dotted curve indicates the concentration of H, which also increases in that region. Therefore, an enhancement of doping of both Zn and H were discovered with the use of Sb as surfactant.

This new technique has a lot of advantages over the codoping and ion beam implantation that were discussed above. The surfactant always stays on the top of the expitaxial surface and does not incorporate into the bulk, so it is relatively easy to be removed from the system after the growth. By thermal annealing, the codoped H is easy to remove and the p-type dopant, Zn, will stay in the bulk. There could be various physical mechanisms to explain this intriguing technology advance. The presence of the surfactant(s) may lower the doping energy of Zn thermodynamically. Or it (they) may enhance the diffusion of Zn into the bulk. However, the lack of *in situ* observation of the epitaxial surface makes it difficult to study the underlying physical mechanism of the surfactant enhanced doping, because it is usually impossible to observe the epitaxial surface during OMVPE growth. Also, H as a surfactant or codopant is difficult to observe directly. To study this problem, we have to make some guesses about the surface, including elements on the surface and surface reconstructions. In the past 20 years, due to the improvement of computing theory, algorithm and parallel-computing technique, DFT has been proved as an effective tool to study structural, electronic and transport properties of various semiconductor systems. Work done by DFT on III-V semiconductors gives

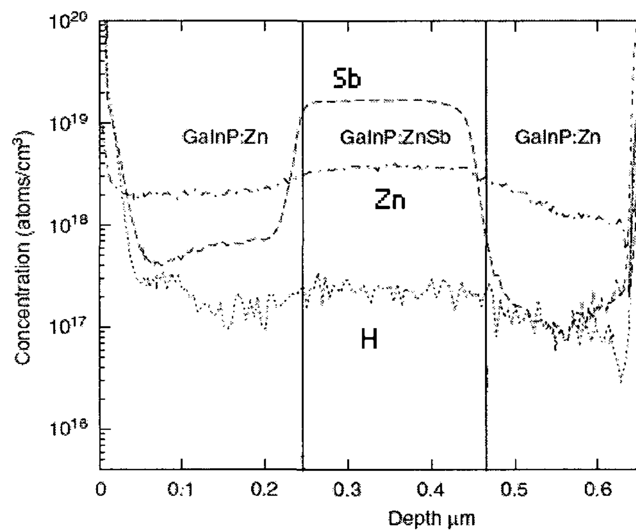

Fig. 1.3. SIMS depth profile of Zn-doped GaInP. The Zn flow was kept constant for the entire growth while a small amount of TESb was added to the system only during the middle layer growth. Zn and H concentrations increase when Sb is present. The positions of the individual interfaces are indicated . (Adapted from Reference [9].)

good agreement with experiments, such as studies of surface reconstructions of III-V semiconductors [14], doping [10,11], surfactant effects, etc. [15]. The results of DFT studies are more and more widely accepted by semiconductor experimentalists. Therefore, DFT calculations can be an effective tool to study the surfactant enhanced doping problem.

Before attacking the doping problem, a brief introduction of surfactants and surfactant-related phenomena in epitaxial growth will be provided, which may help understand the role of surfactant in the doping.

1.3. Review of surfactant effects

Surfactant is the mixed form of "**surf**ace **act**ive **agent**"[16]. Surfactants can reduce the interface tension between oil and water and allow oil and water to mix. Therfore, soap and detergent are the primary surfactants. In this sense, the history of surfactant can be traced back to the era of ancient Babylon about 5000 years ago. At that time, people boiled fats with ashes to make soap-like materials, although they did not use them for soap purposes, but for hair styling aids [17]. Surfactants are also widely used in the cosmetics industry.

The use of surfactants in semiconductor epitaxial growth can be traced back to 20 years ago. Copel etal. introduced the concept of surfactant into epitaxial growth in 1989 [18]. They demonstrated the important role of As as a surfactant in the Ge growth on Si(001) and Si on Ge/Si(001) growth[18]. With the presence of As in the system, the island formation of Si on Ge/Si(001) can be suppressed [18]. Fig 1.4 (a) shows the backscattering spectra for a nonchanneling geometry for Ge/Si(001) without As [18]. Fig 1.4 (b) shows the case with As.

This work attracted vast research interest on the role of surfactants in epitaxial growth, largely because surfactant in epitaxial growth can lower the surface energy,

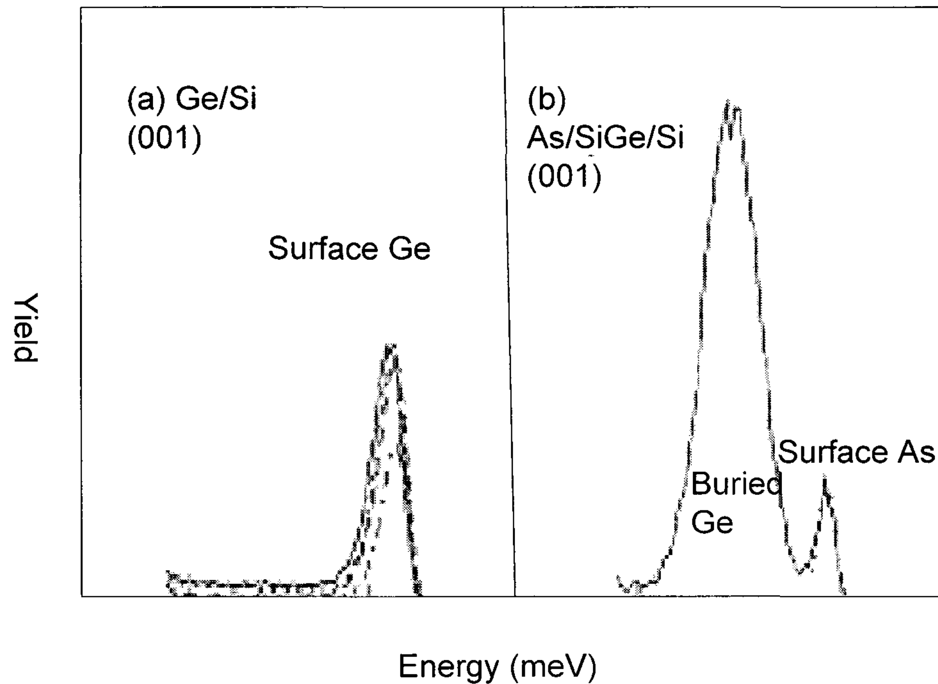

Fig 1.4. Ion backscattering spectra for Ge/Si(001) films grown at 500 C. (a) Deposition without a surfactant results in islanding of Ge after 3 ML, indicated by the tail on the Ge backscatter peak. (b) Films grown with an As passivation layer and capped with 16 ML of Si show no sign of islanding. A 15 – ML Ge film is shown for both random and channeling geometries. (Adapted from Reference [18].)

modify growth mode and often dramatically improve the material and device properties. The surfactant effects can be summarized as the following different categories:

1) Changing the growth mode. For example, Arsenic as a surfactant can change the growth mode of Si/Ge/Si(001) from islanding to layer by layer growth [18]; Sb as surfactant can change the growth mode of Ag on Ag(111) [19]; Te as surfactant can suppress the island formation in InAs[20] and GaInAs [21].

2) Reducing the surface/interface roughness. For example, Bi as surfactant can reduce the surface roughness of InGaAs [22].

3) Suppressing interface alloy intermixing. For example, H as surfactant can suppress the interface mixing of Ge on Si(001) [23].

4) Changing the surface reconstructions, destroying phase ordering of alloys and inducing a new ordered phase. For example, Sb can change the surface reconstruction of GaInP and suppress Cu-Pt ordering in GaInP[24].

5) Enhancing doping, as mentioned above.

The surfactant effects can be attributed to two major physical mechanisms: one is the growth thermodynamics, and the other is the growth kinetics.

In Copel's early work, the growth thermodynamics was investigated [23]. There are three types of thermodynamic growth modes in crystal growth, layer-by-layer growth (known as Frank-Van der Merwe (FV) growth), islanding growth (known as Volmer-Weber (VW) growth) and layer-by-layer growth followed by islanding growth (known as Straski-Krastanov (SK) growth). Fig 1.5 is a schematic illustration of these three growth modes, which are determined by the free energy of the substrate surface (σ_S), the interface energy (σ_i) and the surface free energy of the epitaxial layer. If $\sigma_s \geq \sigma_i + \sigma_f$, FV mode of

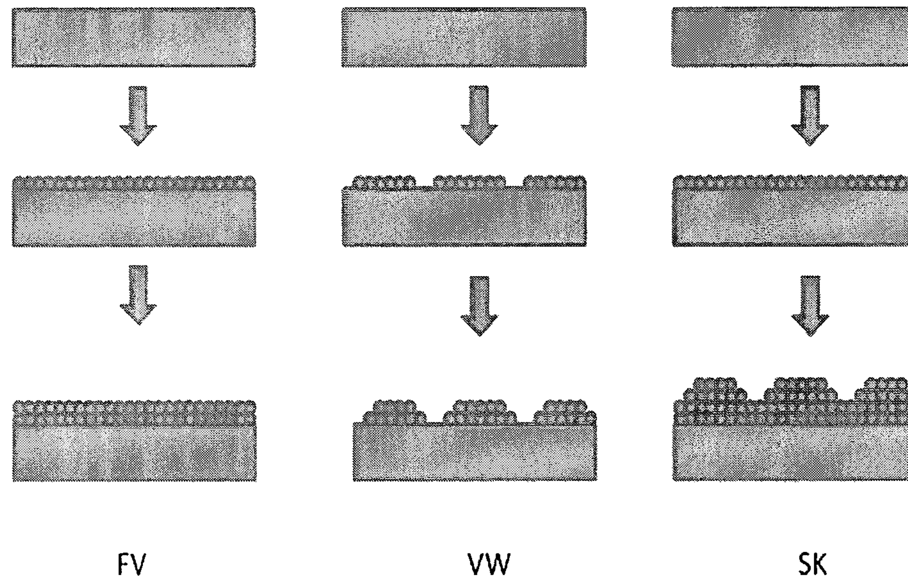

Fig 1.5. Schematic illustration of different growth modes.

growth would occur. If $\sigma_s < \sigma_i + \sigma_f$, VW mode of growth would occur. SK mode of growth occurs when $\sigma_s > \sigma_i + \sigma_f$, but overlayer strain term would later change the direction of the inequality. The basic physical mechanism can be understood in this way: if the free energy of film and interface is lower, the film will fully cover the substrate and FV mode is favored; if the free energy of film and interface is higher, the substrate will be exposed to achieve a lower overall energy and islands are formed. For two materials (heteroepitaxy) , if A can grow on B in a FV or SK mode, then B has to grow on A in an islanding mode. Thus, there is a fundamental barrier to grow a multiple quantumwell kind of embedded structure, because if the embedded film grows well, the cap layer can not follow the same growth mode. In Copel's work, Ge grows on Si(001) in a SK mode, but Si grows on Ge(001) in a VW mode. However, when a layer of As is grown on the surface of Si or Ge, the extra valence electron of As fills the dangling bonds of Si or Ge surface, lowers the surface energy of Si or Ge and forms a stable surface. According to their calculation, the energy of Si/Ge/Si/As is much lower than the energy of Si/Ge/As/Si (2.3 eV per dimer) and the energy of Si/Ge/As is much lower than the energy of Si/As/Ge (1.7 eV per dimer). This suggests that when As covers Si surface and Ge is incorporated into the system, Ge exchanges sites rapidly with As and incorporate into the subsurface. Furthermore, when As covers Ge surface in the Si/Ge film and Si is incorporated into the system, Si would also exchange sites rapidly with As and incorporate into the subsurface and form a good layer-by-layer structure. At the same time, the surface mobility of the growing species decreases rapidly. Therefore, the island formation at the Si/Ge interface is restricted. The role of As in the Si/Ge system is to lower energy of Ge epitaxial layer and keep the inequity of $\sigma_s > \sigma_i + \sigma_f$; the role of As in the Si/Ge/Si system

is to lower the energy of the Si capping layer and also keep the inequity of $\sigma_s > \sigma_i + \sigma_f$ [18].They also performed molecule beam epitaxial (MBE) growth and a medium energy ion scattering (MEIS) measurement to confirm the theory [18].

Thermodynamically, surfactants can also change the surface reconstruction and change the ordering or surface morphology. Ordering is usually determined by the surface. Surface dimers can change the microscopic stress field of the film underneath the dimer, create compressive sites that favor small atoms and tensile sites that favor large atoms, so an ordered structure is due to the surface dimer and surface reconstruction. When surfactants are incorporated, the surface reconstructions are changed. Ordering of alloys is therefore changed or eliminated. In 1999, Sb as an isoelectronic surfactant during the growth of GaInP was studied. Sb replaces the P dimer and also eliminates the ordering in GaInP [24,25]. Bi as an isoelectronic surfactant can also change the surface structure of GaInP and eliminate ordering [26]. A large amount of surfactant Sb can also change the surface reconstruction of InGaP from 2x4 to 2x3 and induce a triple period ordering structure in GaInP[24]. Pillai et al. reported that the change of surface reconstruction may also influence the surface (interface) morphology [22]. They studied the $In_xGa_{1-x}As$/GaAs heterostructure with Bi as a surfactant. (Bismuth is also a good candidate for surfactant, because it is difficult to incorporate Bi into III-V semiconductors during epitaxial growth.) In their experiment, they found the surface reconstruction is changed from 2x4 to 1x3. The surface roughness decreased when Bi surfactant is incorporated into the system. Also, Bi slightly reduces the interface widths. Therefore, Bi as surfactant can improve the structural and optical quality of InGaAs/GaAs structures [22].

Although there is a thermodynamic driving force to suppress the island formation as early surfactant research indicated, some experiments, such as molecule beam epitaxy, are often performed far from equilibrium. Later studies indicated that growth kinetics is also very important for surfactant effects. Surfactants may reduce the surface diffusion and change the growth mode [23].

There is a large amount of atomic H in the growth chamber of OMVPE. Infrared spectroscopy found that the H may attach to P surface dimers and change the surface reconstruction from 2x4 to 2x2 [27]. Therefore, it is essential to study the role of H in semiconductors as surfactants. H as a surfactant can also play an important role in epitaxial growth. H can change both the growth thermodynamics and kinetics. In 1998, Rudkevich et al. reported that a reversible place exchange between Ge and Si on Ge-covered Si(001) when the surface is covered with atomic H [23]. The surface H induces Si surface segregation in a growth front consisting of Si, Ge and H. First-principles calculations were performed to confirm a thermodynamic driving force for this place exchange. The role of H is to saturate the dangling bonds of Si and Ge. Because Si-H bond is stronger than Ge-H, Si-H terminated surface is energetically favorable [23].

Surfactant-mediated growth is often highly complicated. Both thermodynamics and kinetics may play important roles in the improvement of structural and device properties. In this thesis, the thermodynamic part of the surfactant enhanced doping effect will be studied. However, kinetic effects can be as important as thermodynamics effects, which is beyond the scope of this thesis.

All the surfactant effects listed above are only involved with **one element**. In this thesis, based on our DFT study, we discovered an intriguing **dual surfactant effect,**

which will be covered in the following chapters. We found that both Sb and H play important roles in the doping enhancement of Zn. When either Sb or H is incorporated as a surfactant, the doping energy of Zn does not decrease. The doping energy of Zn is reduced greatly only when both Sb and H are incorporated as surfactants.

1.4. Electron counting model

The first step to study this intriguing dual surfactant effect is to revisit the process of doping to understand the general doping phenomena. According to the definition of semiconductor doping, the dopant element is normally either one electron less or one electron more than the host element it replaces. Suppose the host lattice is stable before doping, when a dopant is incorporated into the host lattice, the balance of the electron distribution is broken and the lattice suffers from either electron shortage or excess electrons and becomes unstable. There is a general model to determine whether a semiconductor surface (bulk) is stable due to the distribution of electrons, which is called electron counting model.

The concept of electron counting model to study the GaAs surface reconstruction was first introduced by Pashley in 1989. It was found by STM that during MBE growth, the surface reconstruction of GaAs is a 2x4 structure with a missing dimer, as shown in Fig. 1.6 [28]. Total energy calculation also confirmed that this structure has the lowest energy [29]. Pashley claimed that this low energy structure can be understood using a simple electron counting model and verified that all the principle reconstructions of low index plains of GaAs can also be explained by the electron counting model [28].

Because the bonds of GaP , like that of GaAs and other III-V semiconductors, are

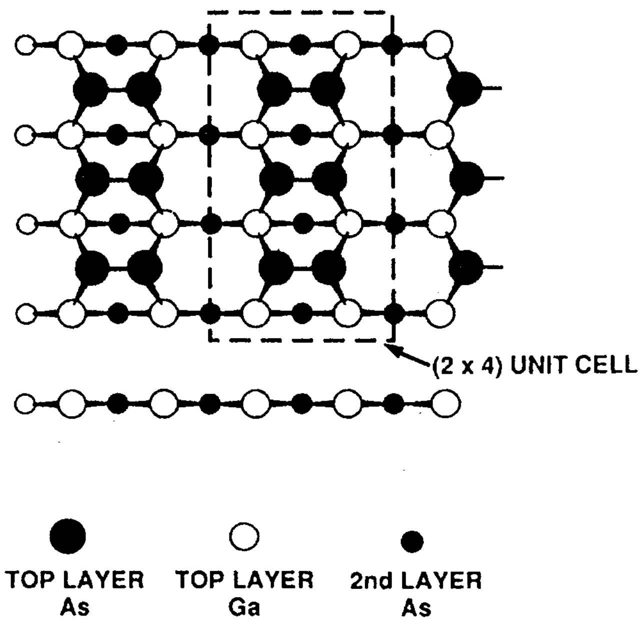

Fig 1.6. The missing dimer structure of GaP surface reconstruction. (Adapted from Reference [26].)

sp^3 hybridized, the surface reconstruction of GaP is similar to that of GaAs. Two hybridized orbits from Ga and P combine to form a bonding and antibonding orbital in the bulk. However, on the surface, some hybrid orbits can not form bonds. If there is no surface reconstruction, those partially filled bonds (i.e., the dangling bond) will remain on the surface. The dangling bonds of the cation (Ga) will be in the conduction band and the dangling bonds of the anion (P) will be in the valence band. These are high energy configurations. In order to lower the total energy, the dangling bond for the cation (Ga) should be empty and the dangling bond for the anion (P) should be filled. If this condition is satisfied, the surface of GaP is semiconducting. If the conduction band is partially filled, the surface is metallic. The electron counting model can be described as the following [28]: the lowest energy configuration is achieved when anion's dangling bonds are filled and cation's dangling bonds are empty.

Now let's apply the electron counting to a P terminated surface of GaP without H, which is often the configuration of MBE. The surface atoms often tend to form dimers to eliminate dangling bonds. Since the valence of P is 5 and the valence of Ga is 3, for each GaP bond, P provides 5/4 electrons and Ga provides ¾ electrons. According to electron counting model, those surface anion (P) dimers have to be filled with electrons to achieve a low energy surface. For each dimer, the number of electrons required is 11 electrons for each dimer (two for the dimer bond, two for each lone pair of P and 5/4 * 4 = 5 (there are 4 GaP bonds and for each bond, P contributes 4/5 electrons) bonding to lower layer). Each anion (P) dimer can provide 10 electrons. Therefore, the surface of GaP can not be fully covered by P dimers, because there is one electron shortage for each dimer. To supply the extra electron to each surface dimer, there must be missing P dimer(s) so that

metallic Ga can provide the extra electrons. For a 2x4 unit cell with one missing P dimer, there are 4 Ga atoms exposed, as shown in Fig. 1.6. Each Ga atom's dangling bond has to be empty to satisfy electron counting. Since each Ga atom has one dangling bond, which provides ¾ electron, 4 Ga atoms can thus provide 3 electrons to surface P dimers to fill up the dangling bonds of 3 P dimers. Therefore, a stable GaP surface without H has the 2x4 reconstruction with one missing dimer, as shown in Fig. 1.6. This simple calculation agrees with the STM image and the total energy calculation. This model can also be extended to group II and group VI semiconductor compounds and group IV semiconductors. Despite the seemingly complicated counting above, the electron counting model indicates a very simple and general rule for semiconductor surfaces. The semiconductor surface can not be a stable surface if dangling bonds of any anions are not fully filled and the dangling bonds of any cations are not empty.

For the InGaP/GaP system we mentioned above, the surface reconstruction for the (001) surface without H is 2x4 with one missing dimer. However, due to a large amount H existing in the OMVPE growth chamber, those H would adsorb onto the surface dimer and therefore change the surface reconstruction. Each H can provide one extra electron to the system for electron counting purposes. According to the discussion above, each P dimer needs one extra electron, so the H can provide that extra electron and attach to the dimers in alternative sites to give the lowest energy configuration, which is 2x2, as shown in Figure 1.7. Those dimer bonds would form buckling structures instead of flat ones due to Jahn-Teller distortion effect to achieve the lower energy.

This 2x2 (2x2) surface reconstruction of InP was confirmed by infrared spectroscopy by Chen et al. [30]. They analyzed the infrared spectra of InP (001) surface

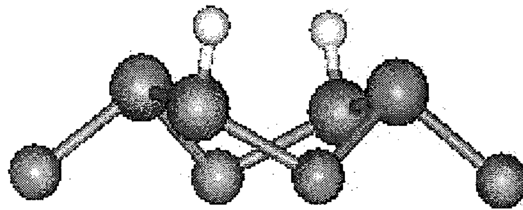

Fig 1.7, Schematic illustration of a 2x2 surface reconstruction for GaP with H adsorbed on top dimers. Small (white): H; Large (Orange): P; Medium (purple): Ga.

and found a sharp P-H stretching mode at 2308 cm^{-1}. Based on their DFT calculation, this mode results from a single H atom bonded to one end of the buckled dimer. Therefore, in our future calculation of Zn doping in GaP system, a super cell containing the 2x2 surface reconstruction will be used, which will be further discussed in Chapter 3.

The electron counting model is not only important in surface reconstruction analysis, but also can provide physical understanding for doped systems. Because the dopant element has either one electron less or one electron more than the host element it replaces, the doping process can never satisfy the electron counting model without any foreign compensation electrons. That's also the intrinsic difficulty of doping. Thus, one possible strategy to enhance doping can be to help the system satisfy electron counting in a certain degree in the doping process. For example, we can provide extra electrons for p-type doping, so that the electron counting model can still be satisfied after doping. As we mentioned above, H in the OMVPE growth chamber or the codoped n-type dopants can serve that purpose as a source of electrons. Or we can provide relatively more metallic elements into the system which serve as "electron reservoirs" to enhance doping. The interaction between electrons and cores of metallic elements is relatively weak, so when the electron counting model is broken due to the doping processes, these elements tend to provide more electrons to help electron redistribution comparing with less metallic elements. The codoping process can be a possible example of this. When the highly metallic In atoms coupled with 2 N atoms are doped into ZnSe, although one N (p-type dopant) is neutralized by In, the high metallic In would still serve as a possible electron reservoir to provide more electrons into the system to assist electron redistribution. All

discussions here are still hypothetical, which need to be examined by DFT calculations, which will be discussed in following chapters.

Also, if the hypothesis above is valid, the choice of surface reconstruction may not be critical to understanding this problem, because the methods to satisfy the electron counting model in a certain degree during the doping process may not be dependent upon which surface reconstruction we choose in our calculation as long as they satisfy electron counting. So before the doping, the surface satisfies the electron counting and is a low energy surface. During the doping process, the electron counting model is broken, and the electron source (either the foreign codopants or the metallic surfactant) would help the system to fully or partially satisfy the electron counting model. So the key in our choice of the surface is to satisfy electron counting model. Although there could exist other low energy surfaces, as long as they also have to satisfy the electron counting model, our general discussion is still valid. For this reason, we believe the dual surfactant effect we discuss above can be a general doping strategy for all III-V or II-VI wide band gap semiconductors, because its principle is surface reconstruction (as long as the surface reconstruction satisfies the electron counting model as electron counting model stated) or lattice independent.

1.5. References

[1] J. R. Woodyard, US Patent 2530110, (1944).

[2] J. Bardeen, Summit, and W. H. Brattain, US Patent 2524035, (1948).

[3] S. Nakamura, J. Vac. Sci. Technol. A **13,** 705, (1995).

[4] I. Akasaki, S. Sota, H. Sakai, T. Tanaka, M. Koike, H. Amano, Electron. Lett. **32** 1105, (1996).

[5] P. Perlin, I. Gorczyca, N.E. Christansen, I. Grzegory, H. Teisseyre, T. Suski, Phys. Rev. B **45,** 13307, (1992).

[6] D. B. Laks, C.G. Van de Walle, G. F. Neumark, P. E. Blochl, S. T. Pantelides, Phys. Rev. B **45,** 10965, (1992).

[7] T. Tanaka, A. Watanabe, H. Amano, Y. Kobayashi, and I. Akasaki, Appl. Phys. Lett. **65**, 593, (1994).

[8] W. Walukiewicz, Physica B: Condensed Matter **302-303**, 123, (2001).

[9] D.C. Chapman, A.D. Howard and G.B. Stringfellow, Jour. of Crys. Growth, **287,** Issue 2, 647, (2006).

[10] Katayama-Yoshida, Yamamoto, Phys. Stat. Sol. (b) **202**, 763, (1997).

[11] S. B. Zhang, S. -H. Wei and Yanfa Yan, Physica B: Condensed Matter **302-303**, 135, (2001).

[12] Alan Mills, III-Vs Review, **14**, Issue 5, 28, (2001).

[13] J.K. Shurtleff, S.W. Jun, G.B. Stringfellow, Appl. Phys. Lett. **78** (20), 3038, (2001).

[14] Chris G. Van de Walle, and J. Neugebauer, Phys. Rev. Lett. **88**, 066103, (2002).

[15] R. Wixom, N. A. Modine, and G. B. Stringfellow, Phys. Rev. B **67,** 115309, (2003).

[16]In Merriam-Webster Online Dictionary, from http://www.merriam-webster.com/dictionary/surfactant, (2009).

[17] M. Willcox (2000). "Soap". in Hilda Butler. Poucher's Perfumes, Cosmetics and Soaps (10th edition ed.). Dordrecht: Kluwer Academic Publishers. pp. 453, (2000).

[18] M. Copel, M. C. Reuter, Efthimios Kaxiras, and R. M. Tromp, Phys. Rev. Lett. **63**, 632, (1989).

[19] G. Rosenfeld, R. Servaty, C. Teichert, B. Poelsema, and G. Comsa, Phys. Rev. Lett. **71**, 6, (1993).

[20] N. Grandjean, J. Massies, and V. H. Etgens, Phys. Rev. Lett. **69**, 796, (1992).

[21] Grandjean, J. Massies, C. Delamarre, L. P. Wang, A. Dubon, and J. Y. Laval, Appl. Phys. Lett. **63**, 66, (1993).

[22] M. R. Pillai, Seong-Soo Kim, S. T. Ho, S. A. Barnett, J. Vac. Sci. Technol. B **18**, 1232, (2000).

[23] E. Rudkevich, Feng Liu, D. E. Savage, T. F. Kuech, L. McCaughan, and M. G. Lagally, Phys. Rev. Lett. **81**, 3467, (1998).

[24] C. M. Fetzer, R. T. Leed, J. K. Schurtleff, G. B. Stringfellow, S. M. Lee and T. Y. Seong, Appl. Phys. Lett. **76**, 1440, (2000).

[25] J. K. Shurtleff, R. T. Lee, C. M. Fetzer, and G. B. Stringfellow, Appl. Phys. Lett. **75**, 1914, (1999).

[26] S. W. Jun, G. B. Stringfellow, J. K. Shurtleff and R. T. Lee, Journal of Crystal Growth Volume **235**, Issues 1-4, (2002).

[27] Li L, Fu Q, Li CH, Han BK, Hicks RF, Phys. Rev. B **61**, 15, (2003).

[28] M. D. Pashley, Phys. Review. B **40**, 10481, (1989).

[29] D. J. Chadi, J. Vac. Sci. Technol. A **5**, 834, (1987).

[30] G. Chen, S. F. Cheng, D. J. Tobin, L. Li, K. Raghavachari, and R. F. Hicks, Phys. Rev. B **68**, 121303, (2003).

CHAPTER 2

METHODOLOGY

2.1. Review of Density-Functional-Theory

To understand the surfactant-enhanced doping introduced in Chapter 1, which is a typical correlated many-body system, extensive first principles calculations based on DFT will be described in this thesis work. It is necessary to give a brief introduction of DFT, which is the most powerful tool to solve quantum mechanical many-body problems. DFT is a theory of correlated many-body systems. The fundamental tenet of DFT is that a functional of the ground state density $n_0(\mathbf{r})$ (a scalar function of position $\mathbf{r}$) determines all the information in the many-body wave-functions for the ground state and all excited states and all the properties of that system [1].

The existence of the functional was proved by Hohenberg, Kohn and Mermin in their early works. In 1964, Hohenberg and Kohn showed that the density can be considered as a "basic variable" and all the properties of the system can be considered to be unique functional of the ground state density [2]. One year later, Mermin extended the Hohenberg-Kohn arguments to finite temperature canonical and grand canonical ensembles [3]. However, the exact functional were not known until today. Also in 1965, Kohn and Sham made their famous ansatz. The Kohn-Sham ansatz provided a useful way to approximate the ground state functional for real systems of many electrons [4]. Kohn and Sham's formulation of DFT has become the basis of most of modern DFT calculation

methods used today.

The DFT of quantum systems was first proposed by Thomas and Fermi in 1927 [5, 6]. They approximated the kinetic energy of the system electrons as a functional of the density, simplified such that the electrons are noninteractive and their density equals the local density at any given point. They both ignored the exchange and correlation among the electrons. In 1930, Dirac extended this work and formulated the local approximation for exchange [7]. In Dirac's work, the energy functional for electrons in an external potential $V_{ext}(r)$ was written as

$$E_{TF}(n) = C_1 \int d^3r n(r)^{5/3} + \int d^3r V_{ext}(r) n(r) + C_2 \int d^3r n(r)^{4/3} + \frac{1}{2} \int d^3r d^3r' n(r) n(r') / |r - r'|, \quad (2.1)$$

where the first term is the local approximation to the kinetic energy, the third term is the local exchange and the last term is the electrostatic Hartree energy [8].

The DFT is much simpler than the many-body Schrodinger equation, which includes 3N degrees of freedom for N electrons. However, the Thomas-Fermi approach neglected the exchange and correlation and missed important physics, such as shell structures of atoms and binding of molecules. Therefore, this approach is too rough and is not accurate enough to describe the electrons in matter.

In 1964, Hohenberg and Kohn formulated the DFT as an exact theory of many-body systems [2]. The Hamiltonian of any system of interacting particles under an external field can be written as [2]:

$$\hat{H} = -\frac{\hbar^2}{2m_e} \sum_i \nabla_i^2 + \sum_i V_{ext}(r_i) + \frac{1}{2} \sum_{i \neq j} \frac{e^2}{|r_i - r_j|}. \quad (2.2)$$

The three terms are the kinetics energy, external potential and electron and electron interaction term in order. The relations established by Hohenberg and Kohn can be stated as [2]:

Theorem I: Suppose a system consisting of interacting particles under an external potential $V_{ext}(\mathbf{r})$, the potential $V_{ext}(\mathbf{r})$ is determined by the ground state particle density $n_0(\mathbf{r})$, except for a constant. [9]

Corollary I: Because the Hamiltonian is determined by the ground state particle density, except for a constant, the many-body wave-functions for all states, including the ground and excited states, are determined. Therefore, all properties of the system are determined by the ground state density $n_0(\mathbf{r})$ [9].

Theorem II: A functional for the energy E[n] can be defined, where $n(\mathbf{r})$ is the density. It is valid for any external potential $V_{ext}(\mathbf{r})$. For any particular $V_{ext}(\mathbf{r})$, the ground state energy is the global minimum of this functional. Also, the density $n(\mathbf{r})$ that minimizes the functional is the ground state density $n_0(\mathbf{r})$ [9].

Corollary II: The functional E[n] is sufficient to determine the ground state energy and density. However, excited states of the electrons must be determined by other means. Later work by Mermin showed that thermal equilibrium properties, such as specific heat, are determined by the free-energy functional of the density [9].

The proofs of theorem I and theorem II were given in [10] and will not be included in this thesis.

2.2. The Kohn-Sham ansatz

Because the interacting many-body system is very difficult to solve, it is possible to look for a different auxiliary system to solve this problem easily. The search for such an

auxiliary system is often an educated guess, which is called the "ansatz" in German [1]. In 1965, Kohn and Sham proposed their famous ansatz [4]. They assumed that the ground state density of the original difficult interacting system is equal to the ground state density of a noninteracting system. Therefore, instead of solving the interacting many-body system, people can now solve a set of equations of independent particles that can be solved by numerical means. Still, all the difficult many-body terms are incorporated into an exchange-correlation functional of the density. By solving these equations, one can find the ground state density and energy of the original difficult problem and the accuracy is only limited by the approximation of the exchange correlation functional [4]. The physical insight of the Kohn-Sham ansatz is to replace a difficult problem with an easy one that shares the common answer with the difficult one [1].

The actual calculation is performed on an auxiliary system. The Hamiltonian of the auxiliary system is defined as [4]:

$$\hat{H}^{\sigma}_{aux} = -\frac{1}{2}\nabla^2 + V^{\sigma}(r). \; (2.3)$$

For a system of independent electrons at the ground state, the density and the kinetic energy are respectively [4]:

$$n(r) = \sum_{\sigma} n(r,\sigma) = \sum_{\sigma}\sum_{i=1}^{N^{\sigma}} |\psi_i^{\sigma}|^2 \; , (2,4)$$

$$T_s = -\frac{1}{2}\sum_{\sigma}\sum_{i=1}^{N^{\sigma}} < \psi_i^{\sigma} | \nabla^2 | \psi_i^{\sigma} > = -\frac{1}{2}\sum_{\sigma}\sum_{i=1}^{N^{\sigma}} | \nabla \psi_i^{\sigma} |^2 \, . \; (2.5)$$

The classical Coulomb interaction energy of the electron density n(**r**) interacting with itself is [1],

$$E_{Hatree}[n] = \frac{1}{2}\int d^3r d^3r' \frac{n(r)n(r')}{|r-r'|}. \ (2.6)$$

To rewrite the Hohenberg-Kohn expression of the full interacting many-body problem, Kohn-Sham approach defined the ground state energy as [4],

$$E_{KS} = T_s[n] + \int dr V_{ext}(r)n(r) + E_{Hartree}[n] + E_{II} + E_{XC}[n]. \ (2.7)$$

Here, $V_{ext}(\mathbf{r})$ is the external potential due to external fields and the nuclei; E_{II} is the interaction between the nuclei. All the many-body effects are grouped into the exchange and correlation function, E_{XC}.

Solution of the Kohn-Sham auxiliary system for the ground state can be viewed as the problem of minimization with respect to the density or effective potential. To apply the Lagrange multiplier method, a set of Kohn-Sham Schrodinger-like equations are derived [4]:

$$\left(-\frac{1}{2}\nabla^2 + V_{ext}(r) + \frac{\delta E_{Hartree}}{\delta n(r,\sigma)} + \frac{\delta E_{XC}}{\delta n(r,\sigma)}\right)\psi_i^\sigma = \varepsilon_i^\sigma \psi_i^\sigma. \ (2.8)$$

This is the famous Kohn-Sham equation. The potential is found self-consistent with the resulting density. It is an exact equation, if the exchange and correlation potential is exact.

The beauty of the Kohn-Sham approach is that it separates the independent particle

kinetic energy and the long-range Hartree terms. Then, the exchange-correlation functional E_{XC} can be approximated as a local or nearly local density [4].

Kohn and Sham showed in their seminal paper that the exchange and correlation function is generally local for solids, because solids can often be viewed as close to the limit of homogeneous electron gas [4]. Thus, they proposed the local spin density approximation, so that the exchange correlation energy is an integral over all space with the exchange correlation energy density at the point assumed to be the same as in a homogeneous electron gas with the same density [11]. The detailed discussion of the local density approximation is beyond the scope of this thesis.

2.3. Solving the Kohn-Sham equations

A straightforward way to solve the Kohn-Sham equations is to follow the condition that the effective potential and the density are consistent, i.e., to obtain a self-consistent solution. The first step is to make an initial guess of the density first, then calculate the corresponding effective potential and solve the Kohn-Sham equations; from the results, the new electron density can be calculated; if the density and the effective potential are consistent, the energy, force, stresses, eigenvalues etc. can be achieved and the calculation is done; otherwise, the effective potential can be recalculated based on a linear combination of previous densities and the process is repeated. In this step, a so-called steepest decent method can be applied to find the minimized energy [12]. Fig. 2.1 shows the schematic representation of the self-consistent loop for solutions of Kohn-Sham equations [13].

To solve the Kohn-Sham equations, a basis set needs to be chosen. There are two types of basis sets: one is based on plane waves, the other is based on localized orbits.

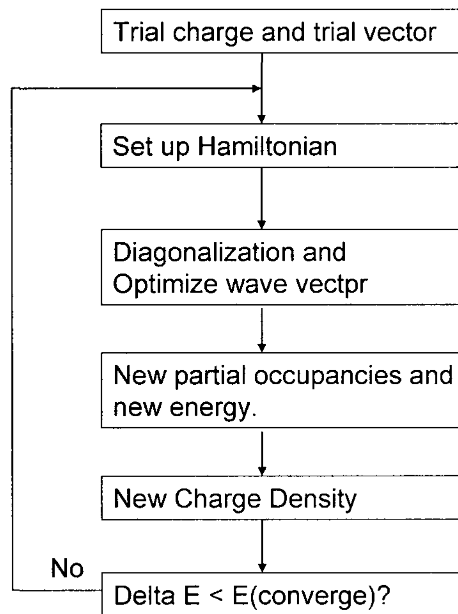

Fig 2.1, Calculation of Kohn Sham ground state. (Adapted from Reference [13].)

Plane waves and grids are two major methodologies to solve differential equations. Plane waves are especially appropriate for periodic crystals calculation and localized orbits (grids) are suitable for finite systems. In modern electronic structure calculations, both methods are extensively applied with fast Fourier transformation [14].

2.4. Pseudopotential

To achieve accurate electronic calculation results, the Coulomb potential of the nucleus and the effects of the core electrons need to be included. In this sense, an all electron calculated potential is necessary. However, the Coulomb potential of the nucleus is usually strong and the core electrons are usually tightly bound, which usually results in a high kinetic energy and a lot of terms in Fourier transform that affect the calculation efficiency. Also, the core electrons have a small effect in valence electron bonding. One way to improve the calculation efficiency is to replace all electron calculated potential with a so-called "pseudopotential" [15]. Instead of solving the difficult problem of the Coulomb potential of the nucleus, an effective ionic potential acting on the valence electrons can be calculated [15]. This potential is called pseudopotential. A pseudopotential can be generated in an atomic calculation and the calculation result can be the input of calculations of properties of valence electrons in solids or molecules, because the core states almost remain unchanged in these situations [15], except for some extreme conditions, such as very high pressures. Pseudo-potentials can usually be constructed in two parts: the local (l-independent) part plus the nonlocal (l-dependent) part (l is the orbit quantum number)[15]. To preserve the right physics of the all electron case, pseudo-potentials usually satisfy a so-called norm conserving condition: the eigenvalues and the orbits are required to be the same for the pseudo and the all electron

case for $r>R_c$, each potential $V_l(r)$ equals to the local (l-independent) all electron potential and $V_l(r) \rightarrow Z_{ion}/r$ for $r \rightarrow \infty$ [15]. Fig. 2.2 shows a schematic illustration of a pseudo-potential [15].

The ab-initio norm-conserving and ultra-soft pseudopotentials are the basis of the accurate electronic calculations [16]. One goal of creating potential is to make the potential as smooth as possible, because in plane wave calculations, the potential is expanded in Fourier components and the performance of the calculation is to the power of the number of Fourier components [16]. One way to achieve the smoothness is to introduce the concept of "ultra-soft pseudopotentials"[16]. "Ultra-soft pseudopotential" is a practical approach for solving equations beyond the applicability of those formulations [15]. The concept of ultra-soft pseudopotential was proposed by Blochl and Vanderbilt [16,17]. They rewrote a nonlocal potential in a form involving a smooth function that is not norm conserving [16, 17]. Fig. 2.3 [15] shows a schematic illustration of an all electron calculated wave function (solid line), a norm conserving pseudo-potential calculated one (dotted) and an ultra-soft pseudo-potential calculated one (dashed). As we can see, the ultra-soft pseudo-potential yields the smoothest wave function among the three and is the most efficient in calculation.

In this thesis, Vienna ab-initio simulation package (VASP) [18] is used to calculate the doping energy of various dopants in GaP. VASP is a complex package for ab-initio quantum-mechanical molecular dynamics (MD) simulations using pseudopotentials or the projector-augmented wave method and a plane wave basis set [18]. VASP is the most widely used DFT simulation package, which runs well in parallel computers. In our calculation, we chose the ultra-soft pseudopotential method within the local density

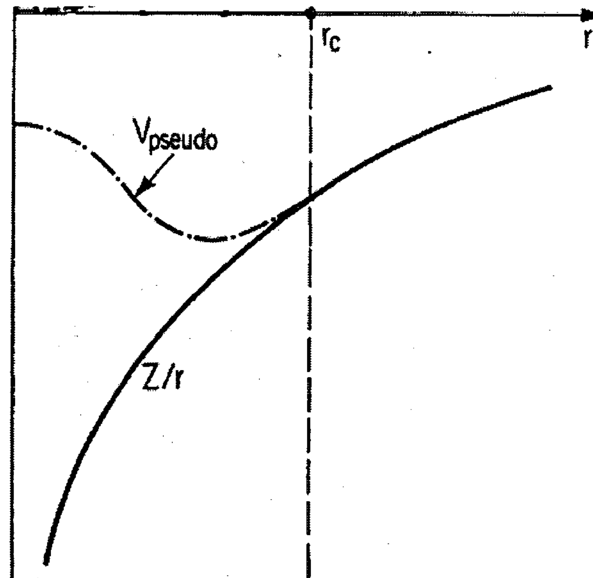

Fig. 2.2, Schematic illustration of a pseudo-potential. (Adapted from Reference [15].)

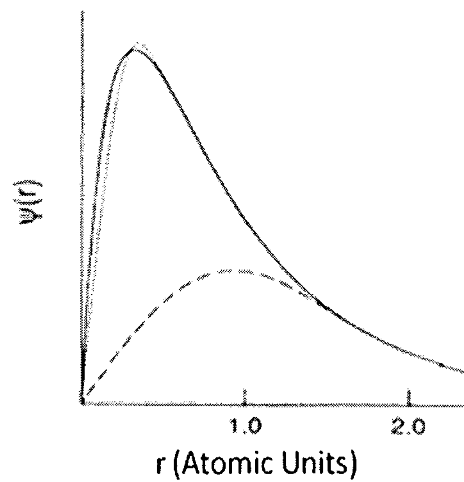

Fig. 2.3, Schematic illustration of an all electron calculated wave function (solid line), a norm conserving pseudo-potential calculated one (dotted) and an ultra-soft pseudo-potential calculated one (dashed).(Adapted from Reference [15].)

approximation as the exchange-correlation functional.

2.5. Supercell technique and simulation set-up

In this thesis, a super cell technique is applied to simulate the thin films using a truncated slab.

As briefly discussed in Chapter 1, under OMVPE growth conditions, H decomposed from the P precursor covers the (0 0 1) surface of InP [19]. The H coverage converts the surface into a (2x2) reconstruction as observed by STM[19]. Therefore, we choose a (2x2) reconstructed surface in our calculation of GaP, as shown in Fig. 2.4 [20]. A periodic boundary condition is applied along x,y,z directions. The super cell slab consists of 4 layers of Ga atoms and 5 layers of P atoms. The top surface is terminated by P atoms, which agrees with the P rich OMVPE growth condition. The bottom two atomic layers are fixed at their bulk position. The bottom layer of P is passivated by ¾ charged H atoms to saturate the dangling bonds of the P atoms, because according to electron counting rule, each P contributes 5/4 electron to each bond and needs ¾ electrons to saturate. There is a so-called "dimer bucking" on the top surface, as discussed in Chapter 1. Each surface H atom attaches to the lower P atom of the buckled dimer to give the lowest energy as confirmed by our calculations.

We performed a series of bulk energy calculations and obtained 5.4 Å as the lattice parameter for the GaP slab. The plane wave cut-off energy we chose is 348 eV, following the recommendations of VASP generated pseudopotentials and convergence tests of different cut-off energy configurations. To model the thin film, a vacuum layer needs to be included. We choose a 12.8 Å vacuum layer after the convergence tests of a series of different vacuum layer configurations. We choose 4x4x1 k-point mesh for Brillouin

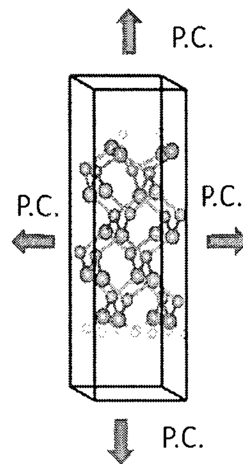

Fig. 2.4, Schematic illustration of GaP supercell slab. Large sphere: P; small sphere: Ga; smallest sphere: H. (Adapted from Reference [20].)

zone sampling following the convergence tests of 4x4x1 , 7x7x1 and 10x10x1 k-point meshes. The energy minimization was performed by relaxing atomic positions until the forces converged to less than 0.1 meV/Å.

In experimental setups, millions of atoms are involved in the growth front. In the DFT calculation, only less than a few hundreds of atoms can be calculated due to the nature of highly intensive DFT calculations and the limit of performance of current parallel computers. The doping concentration in our calculation is to the order of $10^{21}/cm^3$, which is higher than the experimental results[9]. Therefore, the related doping energy calculation may only qualitatively reflect the physical essence of the experimental results.

2.6 References

[1] R. M. Martin, Electronic Structure Basic Theory and Practical Methods, Cambridge University Press, pp. 119, (2004).

[2] P. Hohenberg and W. Kohn, Phys. Rev. **136**, B. 864, (1964).

[3] N. D. Mermin, Phys. Rev. **137**, A1441, (1965).

[4] Kohn and L. J. Sham, Phys. Rev. **137**, A1697 (1965).

[5] L. H. Thomas, Proc. Cambridge Phil. Roy. Soc. **23**, 542, (1927).

[6] E. Fermi, Rend. Accad. Naz. Lincei **6**, 602, (1927).

[7] P. A. M. Dirac, Proc. Cambridge Phil. Roy. Soc. **26**, 376, (1930).

[8] R. M. Martin, Electronic Structure Basic Theory and Practical Methods, Cambridge University Press, pp. 120, (2004).

[9] R. M. Martin, Electronic Structure Basic Theory and Practical Methods, Cambridge University Press, pp. 122, (2004).

[10] R. M. Martin, Electronic Structure Basic Theory and Practical Methods, Cambridge University Press, pp. 123, (2004).

[11] R. M. Martin, Electronic Structure Basic Theory and Practical Methods, Cambridge University Press, pp. 153, (2004).

[12] R. M. Martin, Electronic Structure Basic Theory and Practical Methods, Cambridge University Press, pp. 172, (2004).

[13] G. Kresse and J. Furthmüller, VASP Guide, **9**, 1, (1999), http://cms.mpi.univie.ac.at/vasp/guide/node147.html.

[14] R. M. Martin, Electronic Structure Basic Theory and Practical Methods, Cambridge University Press, pp. 236 and pp. 272, (2004).

[15] R. M. Martin, Electronic Structure Basic Theory and Practical Methods, Cambridge University Press, pp. 204, (2004).

[16] P. E. Blochl, Phys. Rev. B **41**, 5414, (1990).

[17] D. Vanderbilt, Phys. Rev. B **41**, 7892, (1990).

[18] G. Kresse and J. Hafner, Phys. Rev. B **49**, 14251, (1994); G. Kresse and J. Furthmuller, Comput. Matter **6**, 8245, (1994).

[19] Li L, Fu Q, Li CH, Han BK, Hicks RF, Phys. Rev. B **61**, 15, (2003).

[20] J. Y. Zhu, Feng Liu, and G. B. Stringfellow, Phys. Rev. Lett. **101**, 196103, (2008).

CHAPTER 3

DUAL-SURFACTANT EFFECT OF SB AND H ON ENHANCING ZN DOPING IN GAP

A high point of my thesis research is the discovery of a "dual-surfactant" effect on enhancing p-type doping in III-V semiconductors. This new effect was first found for the specific example of dual-surfactants of Sb and H on enhancing Zn doping in GaP, which led to the publication of a research paper in Physics Review Letters [1]. This chapter is a reproduction of this paper. To keep the completeness and flow of the original paper [1], some general discussions on doping, surfactants effect and DFT method in the last two chapters are briefly repeated here. Also, during the preparation of this thesis, one of my Ph.D. committee members, Prof. Virkar, pointed out some mistakes we made in choosing the chemical potential of H in our original calculations [1]. All the calculated energy values associated with the chemical potential of H have been corrected, which are different from those in the original paper [1]. A detailed discussion of how to choose the correct chemical potential of H will be given in Chapter 4.

Surfactants have been widely used in epitaxial growth, as an effective "additional" parameter, to control the thin film microstructure, composition and morphology and hence to improve the thin film properties and device performance. The surfactant effects can be manifest in various forms, including modifying growth mode [2-4], reducing

interface roughness [5], suppressing interface alloy intermixing [6] and enhancing the doping of semiconductors [7-10]. Different physical mechanisms may underlie different surfactant effects, as a surfactant can change growth thermodynamics, such as surface energy and reconstruction [2,6], as well as kinetics, such as surface diffusion [3] and step-edge barriers [4].

A surfactant is defined as an element that floats on top of the growing film surface. (In rare cases, it may also stay in the subsurface region [8].) The role of surfactant is usually considered to be achieved by one single foreign surface element (or chemical species) that is different from the film. Here, we introduce a new "dual-surfactant" effect, for which the role of surfactant can only be achieved by the combined effects of two foreign surface elements while neither of the two can act alone as an effective surfactant. We will demonstrate the dual-surfactant effect for the case of enhancing *p*-type doping in III-V semiconductors. The doping of high band gap semiconductors has been a challenging problem for many years. Recently, it has been shown that the use of surfactants provides an effective method for doping of semiconductors [7-10]. Specifically, Sb has been used to enhance doping of Zn into GaInP [9,10]. However, the underlying doping mechanisms remain unclear. An interesting point is that H was observed to be co-incorporated with Zn [9,10]. This has led to the postulate that surface H may also play a role along with surface Sb in the doping process.

We have carried out extensive first-principles calculations of Zn incorporation in the (001) GaP films under the influence of surface Sb and H. We found that Sb alone has little effect on the doping energy of Zn in GaP, and it is only when H is also present that the Zn doping energy is substantially lowered by Sb. Also, surface H does not function as

effectively alone without Sb. It is the combined effect of Sb and H that makes the Zn doping process thermodynamically favorable, manifesting a unique dual-surfactant effect. The role of Sb is to serve as an electron reservoir to accommodate the redistribution of electrons, in a similar spirit to the generalized electron counting rule (ECR) in the semiconductor surface with metal elements [11]. The role of H is to supply two electrons to satisfy the ECR for 2x2 surface reconstruction and one extra electron missing from the *p*-type dopant, so that the system can satisfy the ECR [12].

Our calculations were performed using the VASP code [13] within the local density approximation. We model the GaP (001) films by a supercell slab consisting of 4 layers of Ga and 5 layers of P atoms, plus a 12.8 Å vacuum layer. The bottom two atomic layers were fixed at their bulk positions with the last layer of Ga passivated by 3/4 charged H. We used a plane wave cutoff energy of 340 eV and a 4×4×1 k-point mesh for Brillouin zone sampling. Total energy minimization was performed by relaxing atomic positions until the forces converged to less than ~ 0.1 meV/Å.

To obtain the Zn doping energy, we replace one Ga atom in the second (Fig. 3.1) or fourth (Fig. 3.2) atomic layer with a Zn atom, and calculate the energy difference. The effect of surfactant Sb on doping energy was calculated by replacing surface P dimers with Sb dimers. The effect of H as the second surfactant was further studied by introducing different concentrations and configurations of H on the surface. The doping energy is defined as:

$$\Delta E_{\text{doping}} = E_{doped} - E_{undoped} + \mu_{\text{Ga}} - \mu_{\text{Zn}}, \quad (3.1)$$

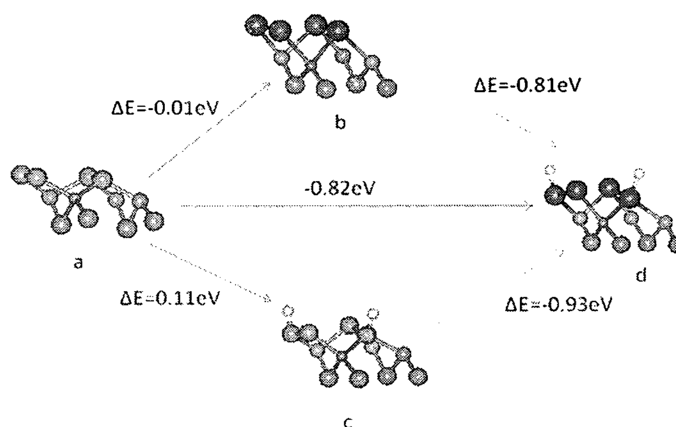

Fig. 3.1. Schematic illustration of various doping configurations, with one Zn atom replacing a Ga atom in the second atomic layer. ΔE indicates the change of doping energy from one configuration to another indicated by the arrows. Largest sphere: Sb; Large sphere: P; medium sphere: Ga; small sphere: Zn; smallest sphere: H.

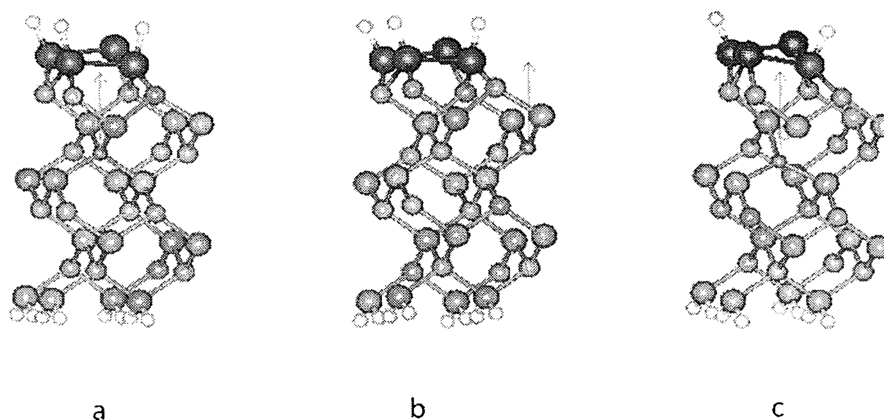

FIG. 3.2. Ball-and-stick schematic illustration of one Zn atom doped in the fourth atomic layer (the second cation layer). Atom labels are the same as in Fig. 3.1. (a) Zn atom doped at the site in between two surface dimers with 3 surface H. (b) Zn atom doped at the site below a surface dimer with 3 surface H. (c) Zn atom doped at the site below a surface dimer with 2 surface H and 1 bulk H next to Zn. (The arrows indicate the position of the Zn atom relative to the surface dimer.)

where E_{doped} ($E_{undoped}$) is the total energy of the doped (undoped) system, i.e., supercell; μ_{Ga} (μ_{Zn}) is the chemical potentials of Ga (Zn). In general, μ_{Ga} may vary from μ_{Ga} [bulk] + ΔH_f [*GaP*] (the *P*-rich condition) to μ_{Ga} [bulk] (the Ga-rich condition) [14], where ΔH_f [*GaP*] is the *GaP* enthalpy of formation; μ_{Zn} equals μ_{Zn} [bulk]. In calculating the change of doping energy due to surfactant Sb, μ_{Ga} and μ_{Zn} would not appear. In the case of H, the doping energy depends on the chemical potential of H (μ_H) if one additional H is added to the system upon doping. We have used the typical value of μ_H= -0.67 eV, one-half of the energy of an H_2 molecule at 900K under 1 atm[15]. [*Note added in this thesis, this value is different from the one used in the original paper. See discussion in the next chapter.*]

The typical reconstruction of clean (001) III/V semiconductor surfaces is (2×4) [16]. However, under OMVPE growth conditions, the presence of H on the surface, from decomposition of the P precursor via the pyrolysis process, converts the surface into a (2×2) reconstruction as observed by STM at room temperature [17], which was deduced to have one H attached to each surface dimer [17] to satisfy the ECR. Therefore, we have used the (2×2)-reconstructed surfaces in our calculations. The authors believe this is reconstruction during OMVPE growth. However, even if this is not, we expect that our results and physical interpretations are still generally applicable, at least qualitatively, to other surface reconstructions of III/V films terminated with group-V dimers and H.

As a reference, we first calculated the Zn doping energy in bulk GaP and obtained $\Delta E_{\mathrm{bulk}} = 2.74\,\mathrm{eV} + \mu_{\mathrm{Ga}} - \mu_{\mathrm{Zn}}$. Then, we calculated the Zn doping energy in the surface positions of a clean GaP (001) film, by replacing the Ga in the second layer, as illustrated in Fig. 3.1a. We obtained $\Delta E^{\mathrm{P}}_{\mathrm{2nd}} = 2.57\ \mathrm{eV} + \mu_{\mathrm{Ga}} - \mu_{\mathrm{Zn}}$, where superscript “P” denotes P-terminated surface and subscript “2nd” denotes Zn dopant position in the second layer.

We found the presence of the surface lowers the doping energy slightly by about 0.17 eV in reference to bulk.

Next, we investigated the surfactant effect of Sb. In experiments, Sb was introduced continuously during OMVPE growth [9,10]. It stays on top of the surface replacing P surface dimers, due to its large atomic size and lower dangling bond energy, which has been demonstrated by surface photo reflection spectra [18] and also supported by previous first-principles calculations [19]. Thus, in our calculations we replaced surface P dimers with Sb dimers. Without H (Fig. 3.1b), we obtained $\Delta E_{2nd}^{Sb} = 2.56\,\text{eV} + \mu_{Ga} - \mu_{Zn}$. Importantly, we found that the Zn doping energy with Sb surface dimers is almost the same as that with P dimers (Fig. 3.1a vs. 3.1b). This indicates that Sb alone does not significantly enhance Zn doping of GaP.

H is inevitably present on the GaP surface during OMVPE growth. Experiments have indicated significant concentrations of H incorporated into the GaP epitaxial film and formation of Zn-H and C-H complexes [8], suggesting that H may play an important role in the process of dopant incorporation. Fundamentally, from a thermodynamic point of view, one significant role H will play is to help the surface satisfy the ECR [11]. Note that the clean GaP(001)-(2×2) model surfaces we discussed above as a reference state does not satisfy the ECR.

The simplest way for the GaP(001)-(2×2) surface to satisfy the ECR is to add one H on each surface dimer on the alternating side, as shown by our calculations to have the lowest energy. The situation remains the same with surfactant Sb (see Fig. 3.1d), as Sb is isoelectronic with P. Thus, to investigate the role of H, we calculated the Zn doping energy with surface H. First, we test the situation with 2 surface H/cell without Sb.

Assuming the H coverage remained the same, with two H atoms before and after Zn incorporation, we found $\Delta E_{2nd}^{\text{P-2H}\rightarrow\text{2H}} = 2.68\,\text{eV} + \mu_{\text{Ga}} - \mu_{\text{Zn}}$. This gives us another important indication that without Sb, H alone does not enhance the doping. In fact, the doping energy with 2 H/cell is 0.11 eV higher than the case without H (Fig. 3.1a vs. Fig. 3.1c). We believe that this is largely because the ECR is satisfied before doping but violated after doping when the ECR would require one additional H/cell.

Next, we investigated the combined effects of Sb and H. Assuming again a surface covered with 2 H/cell before and after Zn incorporation, we found $\Delta E_{2nd}^{\text{Sb-2H}\rightarrow\text{2H}} = 1.75\,\text{eV} + \mu_{\text{Ga}} - \mu_{\text{Zn}}$. Clearly, the Zn doping energy is substantially reduced, by 0.81 eV, relative to the bare Sb-terminated surface without H from Fig. 3.1b to Fig. 3.1d and by 0.93 eV relative to the H-covered P-terminated surface without Sb from Fig. 3.1c to Fig. 3.1d. This observation illustrates the intriguing dual-surfactant effect of Sb and H: the two work together in a constructive manner in terms of lowering the Zn doping energy, while they do not lower the Zn doping energy individually.

The above results indicate that the surfactant effect of Sb is only realized when surface H is also introduced. The underlying physical reason giving rise to the effect of Sb is probably due to the lower electronegativity of Sb in comparison with P. In a similar spirit to the generalized ECR in the semiconductor surface with metal elements proposed recently [11], Sb is more metallic than P, so that Sb can serve more effectively as an electron reservoir to accommodate the redistribution of electrons when a *p*-type dopant is present. Since the *p*-type dopant will violate the ECR by having one less electron, it is easier for Sb than for P to accommodate the missing electron in order to "partially" satisfy the ECR.

The ECR is violated after Zn is doped if the surface remains with 2 H. In order to re-satisfy the ECR, one more H has to be added. This indicates that the Zn doping process is possibly accompanied by H incorporation. To quantify the role of the extra H, we calculated the Zn doping energy by assuming the surface covered with 2 H before but with 3 H after doping (see Fig. 3.2b to 3.2c). We found that $\Delta E_{\text{2nd}}^{\text{Sb-2H}\to\text{3H}} = 0.04\,\text{eV} + \mu_{\text{Ga}} - \mu_{\text{Zn}}$. Clearly, by adding an extra H after doping to satisfy the ECR, the doping energy can be decreased further depending on the H chemical potential (μ_{H}).

The ECR is violated after Zn is doped if the surface remains with 2 H. In order to re-satisfy the ECR, one more H has to be added. This indicates that the Zn doping process is possibly accompanied by H incorporation. To quantify the role of the extra H, we calculated the Zn doping energy by assuming the surface covered with 2 H before but with 3 H after doping (see Fig. 3.2b to 3.2c). We found that, clearly, by adding an extra H after doping to satisfy the ECR, the doping energy can be decreased further depending on the H chemical potential (μ_{H}).

So far, we have shown the dual-surfactant effect of Sb and H in enhancing the Zn doping in the second atomic layer, i.e., the surface position. Next, we examine the possibility of Zn doping into the fourth atomic layer, i.e., the subsurface or "bulk" positions. Based on the above results, we will focus only on the Sb-terminated surface with 2 H before and 3 H after Zn doping. We consider two possible configurations: one with Zn doped in the fourth atomic layer in between two surface Sb dimers (Fig. 3.2a) and the other below the surface Sb dimer (Fig. 3.2b). The respective doping energies are $\Delta E_{\text{4th, between}}^{\text{Sb-2H}\to\text{3H}} = 0.13\text{eV} + \mu_{\text{Ga}} - \mu_{\text{Zn}}$ and $\Delta E_{\text{4th,below}}^{\text{Sb-2H}\to\text{3H}} = 0.21\text{eV} + \mu_{\text{Ga}} - \mu_{\text{Zn}}$. The 0.08 eV

difference between the two reflects the dependence of Zn doping energy on the "atomic-level" stress at these sites [20] and Zn is slightly favored at the tensile sites between surface dimers relative to the compressive sites directly below surface dimers.

Lastly, we have investigated the codoping of Zn and H into GaP. Experiments observed that complexes of Zn, P and H form during doping of Zn in GaP [21]. This suggests some H atoms do not always remain on the surface, but go into the bulk. To examine this possibility, we have calculated the energies associated with one H incorporation into the bulk with Zn, and determined the Zn-P-H complex structures. Figure 3.2c shows the doping of a Zn atom in the subsurface (or bulk) position along with an H atom next to it. There will be 2 H atoms remaining on the surface (in comparison to 3 H in Fig. 3.2b), so that the ECR is still satisfied.

When a surface H goes into the bulk, it changes the Zn bonding configuration in forming a Zn-P-H complex. Without H, the Zn bonds with 4 neighboring P atoms in an *sp*3 hybridization (a tetrahedral structure, Fig. 3.2b). With the extra H, one Zn-P bond is broken to form a P-H bond, and the Zn bonds with 3 neighboring P atoms in an *sp*2 hybridization (a planar structure, Fig. 3.2c). This can also be explained by the ECR. The Zn provides two valance electrons and the H provides one. For both P-H and P-Zn bonds, it takes 3/4 electrons, so their sum gives 3 electrons total to satisfy the ECR. Thus, when H is codoped with Zn, it changes the Zn bonding configuration from *sp*3 to *sp*2 hybridization, forming three Zn-P bonds plus an empty orbital.

The codoping of H with Zn into bulk is also found energetically favorable. The doping energies at the bulk positions forming the Zn-P-H complex are calculated to be $\Delta E_{\text{4th, between}}^{\text{Sb-2H}\rightarrow\text{1 bulk H}} = -0.19\text{eV} + \mu_{\text{Ga}} - \mu_{\text{Zn}}$ for the sites in between surface dimers, and

$\Delta E_{\mathrm{4th,below}}^{\mathrm{Sb\text{-}2H\rightarrow 1\,bulk\,H}} = 0.05\,\mathrm{eV} + \mu_{\mathrm{Ga}} - \mu_{\mathrm{Zn}}$ below surface dimers. Both are lower by 0.2 ~ 0.3 eV than the corresponding cases with all 3 H atoms remaining on the surface. This suggests that there exists a thermodynamic driving force for one H atom to go into the bulk with Zn, i.e. codoping of Zn with H. On the other hand, it is known that H would compensate Zn in bulk GaP, mitigating the doping effect [22,23], which is also confirmed by our electronic structure calculations. To activate the acceptor, annealing can be done after the doping process to remove the H [22,23]. In other words, the co-doped H must be removed after it serves its purpose to assist the Zn incorporation.

Now, based on all the above calculations, we postulate a plausible complete Zn doping process in GaP driven by the dual surfactant effect of Sb and H, as illustrated in Fig 3.3. The doping of Zn in the original P-terminated surface covered with 2 H is shown in Fig. 3.3a. In the first step, with the Sb replacing the P dimers, a Zn atom is doped at the second atomic layer (Fig. 3.3b), where in assisting the doping process, 2 surface H plays the role to satisfy ECR before doping and the Sb plays the role by providing an electron reservoir to accommodate the redistribution of electrons when the ECR is violated after doping. In the second step, one additional H is added to the surface (Fig. 3.3c) to further assist the doping process by adding one more electron to re-satisfy the ECR. In the third step, the Zn atom goes into the bulk and replaces a Ga atom in the fourth or lower atomic layers, and at the same time, a surface H goes together with Zn into the bulk as a co-dopant to form a Zn-P-H complex, as shown in Fig. 3.3d, where the ECR is satisfied both at the surface and in the bulk at the complex site. The corresponding doping energy changes are shown in Fig. 3.4. The first step has ΔE = -0.93 eV, reflecting the role of Sb and 2H as dual surfactants; the second step has ΔE = -1.71 eV, reflecting the role of the third H; the third step has ΔE = -0.23 eV, reflecting the energy gain in forming P-Zn-H complex. Consequently, we have an overall downhill

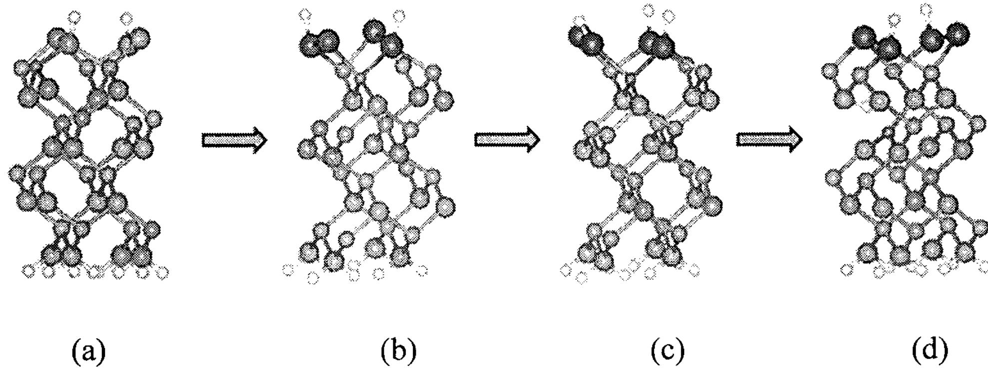

FIG. 3.3. Schematic illustration of a plausible doping process, with one Zn atom replacing a Ga atom in GaP film. Atom labels are the same as in Fig. 3.1. (a) Zn doped into the second atomic layer with surface P dimers. (b) Zn doped into the second atomic layer replacing Ga with surface Sb dimers. (c) One additional H is added onto the surface to re-satisfy ECR. (d) H codoped with Zn into bulk to form a Zn-P-H complex.

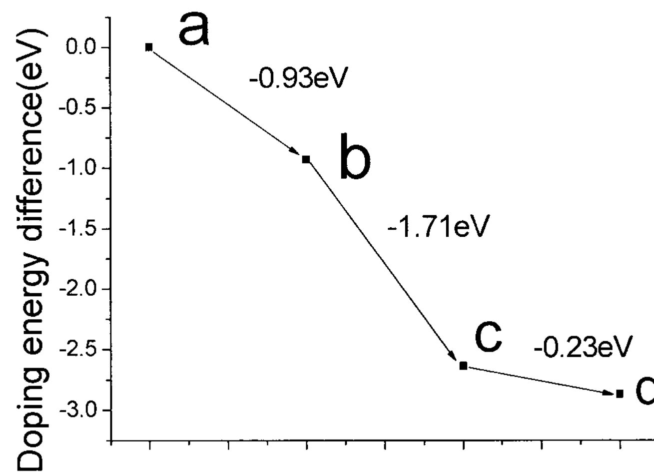

FIG. 3.4. Change of doping energy at each corresponding step as shown in Fig. 3.3.

energy landscape for the whole doping process thermodynamically. Notice that the second-step Zn doping energy with one H added to the system depends on H chemical potential, while the third-step H codoping energy with one H moving from surface to bulk does not. This implies that one may change the partial pressure of H and hence H potential during growth to further enhance Zn doping in the second step without increasing H codoping in the third step.

Our theoretical picture of dual-surfactant effect and its underlying physical mechanism based on the ECR is qualitatively consistent with the experimental observation of both the enhanced Zn doping with Sb introduction during OMVPE growth and the co-incorporation of H with Zn [9,10]. However, because the computation is limited to small cell size, we can only calculate a few representative cases of surface structures, surface coverage, and dopant concentrations. Therefore, the actual energy values may vary with these conditions and should be treated with caution, but the overall trend of the calculated energy changes is expected to be generally correct. Also, other effects, such as temperature and kinetic rates of atom exchange and incorporation, need to be taken into account in the future study in order to obtain a more complete picture of the dual-surfactant effect. For example, from the energy scales shown in Fig. 3.4, temperature is expected to have a lesser effect on the Zn doping energy (~1.0 eV in step 1) then on the H codoping energy (~1.7 eV in step 3), due to the change of chemical potential of H in response to the temperature. However, temperature changes surface H coverage, which will in turn affect doping energy. The kinetic barriers associated with each step of the process are also important, but their calculations would go beyond the scope of this work, which focuses on the thermodynamic aspects of doping energies and

the underlying physical principles based on ECR.

In conclusion, we have discovered an interesting dual-surfactant effect of Sb and H for Zn doping enhancement. The dual-surfactant with two surface elements will greatly broaden the scope and application of the conventional surfactant effect with one surface element. Specifically, in order to accommodate the *p*-type (Zn) dopant incorporation, the role of first surfactant Sb (a "metallic" element) is to provide an electron reservoir to redistribute electrons, while the role of second surfactant H (a "single electron") is to add one electron by each H to help satisfy the ECR. We believe the dual-surfactant effect we disclose here can be used as a general strategy for enhancing *p*-type doping of III-V semiconductors by using a metallic-element with H as dual-surfactants.

The authors are grateful to DOE-BES for supporting this work. The calculations were performed on AMD Opteron cluster at the CHPC, University of Utah.

3.1 References

[1] J. Y. Zhu, Feng Liu, and G. B. Stringfellow, Phys. Rev. Lett. **101**, 196103, (2008).

[2] M. Copel, M. C. Reuter, E. Kaxiras, and R. M. Tromp. Phys. Rev. Lett. **63**, 632, (1989).

[3] G. Rosenfeld, R. Servaty, C. Teichert, B. Poelsema, and G. Comsa, Phys. Rev. Lett. **71**, 895, (1993).

[4] J. Meyer, J. Vrijmoeth, H. van der Vegt, R. Behm, Phys. Rev. B **51,** 14790, (1995).

[5] M. R. Pillai, Seong-Soo Kim, S. T. Ho, S. A. Barnett, J. Vac. Sci. Technol. B **18**, 1232, (2000).

[6] E. Rudkevich, Feng Liu, D. E. Savage, T. Keuch, L. McCaughan, and M. G. Lagally, Phys. Rev. Lett. **81**, 3467, (1998).

[7] C. M. Fetzer, R. T. Lee, J. K. Shurtleff, G. B. Stringfellow, S. M. Lee and T. Y. Seong, Appl. Phys. Lett. **76**, 1440, (2000).

[8] W. Zhu, H. H. Weitering, E. G. Wang. E. Kaxiras, and Z. Zhang, Phys. Rev. Lett. **93**, 126102, (2004)

[9] D. C. Chapman, A. D. Howard, and G. B. Stringfellow, J. Crystal Growth **287**, 647, (2006).

[10] A. D. Howard, D. C. Chapman, and G. B. Stringfellow, J. Appl. Phys. **100**, 44904, (2006).

[11] L. Zhang, E. G. Wang, Q. K. Xue, S. B. Zhang, and Z. Zhang Phys. Rev. Lett. **97**, 126103, (2006).

[12] P. K. Larsen and D. J. Chadi. Phys. Rev. B **37**, 8282, (1988).

[13] G. Kresse and J. Hafner, Phys. Rev. B **49**, 14251 (1994); G. Kresse and J. Furthmuller, Comput. Matter **6**, 8245, (1994).

[14] Chris G. Van de Walle, and J. Neugebauer, Phys. Rev. Lett. **88**, 066103, (2002).

[15] O. Knacke, O. Kubaschewski, K.Hesselmann(Eds.), Thermochemical Properties of Inorganic Substances, Second Edition, Springer-Verlag, pp 803, (1991).

[16] J. A. Appelbaum, G. A. Baraff, and D. R. Hamann Phys. Rev. B **14**, 1623, (1976).

[17] G. Chen, S. F. Cheng, D. J. Tobin, L. Li, K. Raghavachari, and R. F. Hicks, Phys. Rev. B **68**, 121303, (2003).

[18] M. Sugiyama, S. Maeyama, F. Maeda, and M. Oshima, Phys. Rev. B **52**, 2678, (1995).

[19] R. Wixom, N. A. Modine, and G. B. Stringfellow, Phys. Rev. B **67,** 115309, (2003).

[20] Feng Liu and M. G. Lagally, Phys. Rev. Lett. **76**, 3156, (1996).

[21] M. D. McCluskey, E. E. Haller, J. W. Walker, and N. M. Johnson, Appl. Phys. Lett. **65**, 2191, (1994).

[22] E. V. K. Rao, B. Theys, Y. Gottesman, and H. Bissesur, 11th International Conference on Indium Phosphide and Related Materials, 0-7803-5562-8/99 IEEE, (1999).

[23] C. H. Chen, S. A. Stockman, M. J. Peanasky, and C. P. Kuo, Semiconductors and Semimetals, Vol 48, ed. by G. B. Stringfellow, M. G. Craford, Academic Press, pp 122-127, (1997).

CHAPTER 4

DUAL-SURFACTANT EFFECT OF SB AND H ON ENHANCING CATION-SUBSTITUTED P-TYPE DOPING IN GAP

After discovering the dual surfactant effect of Sb and H on enhancing Zn doping in GaP, a natural question is whether such effect is a general phenomenon that can be applied to other dopants. Therefore, I have extended the calculations to several additional p-type dopants including Mg, Be and Cd, which resulted in a second paper on the topic of "dual-surfactant effect" submitted to the Journal of Crystal Growth. This chapter is a reproduction of this paper. To keep the completeness and flow of the original paper, some general discussions on doping, surfactant effect and DFT method are again briefly repeated. In addition, as mentioned in Chapter 3, more extended discussions and corrections of chemical potentials of Ga and H are given in this chapter.

In epitaxial growth, surfactants have been proved to be effective to control the thin film microstructure, composition and morphology and, hence, to improve the thin film properties and device performance. Copel et al. in 1989 first used As as a surfactant in the growth of Si/Ge/Si(001) to suppress island formation [1]. Surfactant effects may affect crystal growth in various forms. They can change the growth mode. In addition to Copel's work [1], the growth mode of Ag on Ag(111) is also changed when Sb is used as a

surfactant [2,3]. Surfactants can reduce interface roughness. For example, Bi as a surfactant reduces the surface roughness of InGaAs grown on GaAs substrates [4]. Interface alloy intermixing can be suppressed by surfactants. For example, H can suppress the interface intermixing of Ge(001) covered Si [5]. They can be used to change the surface reconstruction and, hence, induce the formation of various new ordered phases. For example, Sb is known to suppress Cu-Pt ordering in GaInP [6]. At higher concentrations, it can change the surface reconstruction from (2x4) to (2x3)-like inducing a new ordered phase in InGaP [6]. Surfactants can also strongly affect the incorporation of dopants in semiconductors [7,8]. This last effect will be the focus of this chapter.

The surfactant effects listed above may be attributed to several physical mechanisms. Surfactants can change the growth thermodynamics, by altering the surface energy. For example, surface As is known to lower the surface energy of the Si/Ge/Si system to suppress island formation [1]. In addition to changing the thermodynamics, surfactants can also change the growth kinetics, such as surface diffusion [2] and the size of step-edge barriers [3]. For example, Sb as a surfactant has been shown to reduce the mobility of Ag adatoms. This results in a higher island density leading to a change of growth mode. Sb as a surfactant on Ag (111) or GaAs can also reduce the step edge barrier and promote smoother growth morphologies [3,9].

Obtaining high doping levels in high band gap materials has been a difficult problem for decades. This hinders high-level *p*-type doping in III-V materials such as phosphide and nitride semiconductors. This may be caused by several factors, including the limited solubility of acceptors, H passivation of acceptors, and high acceptor-hole binding energies [10,11]. An effective approach to achieving high p-type doping levels in

GaInP, GaP and GaAs employs the use of surfactants during OMVPE growth [6,7,8]. For example, a recent study showed that Sb can be used to enhance the incorporation of dopants, such as Zn [7,8], and reduce unintentional impurities, such as C, S and Si [8]. In addition to Sb, surface H was postulated to also play a role in the doping process [7,8]. The enhanced Zn doping was speculated to be caused by kinetic and/or thermodynamic factors. The presence of Sb may increase the surface diffusion of Zn and allow more Zn to reach step edges and incorporate into the film [12]. Also, the neutral Zn-H complexes have a lower film doping energy than the isolated Zn [7]. However, there remains insufficient understanding of the underlying doping mechanisms associated with surfactants because it is impossible to directly observe the microscopic doping process.

A surfactant in epitaxial growth is defined as an active element that floats on top of the growing film surface. It is usually a single foreign element. Recently, we introduced a "dual-surfactant" effect, for which the surfactants can assist *p*-type doping of the epitaxial film only when two foreign surface elements are present while neither of the two can act alone to assist doping [13]. Specifically, we studied theoretically the doping process of Zn in GaP and found that the combined effects of Sb and H lower significantly the Zn film doping energy, while neither Sb nor H can work alone as effectively. Here, we use the term "film" doping energy as the energy change for a dopant atom (such as Zn) replacing a cation atom (such as Ga) in the subsurface position during epitaxial growth process to differentiate from the "bulk" doping energy for a dopant atom replacing a cation atom in the bulk. In this paper, we report the results of an investigation of the possible dual surfactant effects of Sb and H on the incorporation of other *p*-type dopants sitting on the Ga sublattice in GaP.

We have carried out extensive first-principles calculations of Zn, Mg, Be and Cd incorporation in (001) GaP films under the influence of surface Sb and H. We found that Sb alone has little effect on the film doping energy of all the dopants in GaP film, and it is only when H is also present that the film doping energy is substantially lowered by Sb. Also, surface H does not function as effectively alone without Sb. It is, thus, the combined effect of Sb and H that makes the *p*-type doping processes thermodynamically favorable. The role of Sb is to serve as an electron reservoir to accommodate the redistribution of electrons, in a similar spirit to the generalized electron counting rule (ECR) in the semiconductor surface with metal elements [14]. The role of H is to supply the one electron missing from the *p*-type dopant, so that the system can satisfy the ECR [15]. Experimentally, it is difficult to achieve high doping levels of Mg and Zn in III-V systems [8,16]. Our findings may illustrate an important theoretical insight and suggest a common strategy for improved *p*-type doping during epitaxial growth in all III-V compounds.

Our calculations were performed using the Vienna *ab initio* simulation package [17] within the local density approximation. We model the GaP (001) films by the same technique as we applied in our previous calculation on the dual surfactant effect of Sb and H on Zn in GaP [13]. We constructed a supercell slab consisting of 4 layers of Ga atoms and 5 layers of P atoms, plus a 12.8 Å vacuum layer (see Fig. 4.1). Also, the vacuum layer allows the film to relax along (001). The bottom two atomic layers were fixed at their bulk positions with the last layer of Ga passivated by 3/4 charged H atoms. We used a plane wave cutoff energy of 348 eV and a 4x4x1 k-point mesh for Brillouin zone sampling. Total energy minimization was performed by relaxing atomic positions

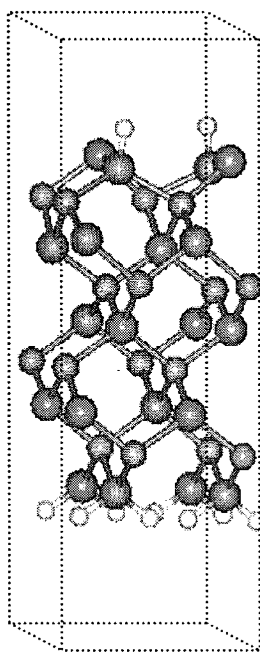

FIG. 4.1. Schematic of GaP supercell slab. Large sphere: P; small sphere: Ga; smallest sphere: H.

until the forces converged to less than ~ 0.1 meV/Å.

In our calculation, we chose the (2x2) reconstructed surface as shown in Fig. 4.1. The typical reconstruction of a clean (001) III/V semiconductor surface is (2×4) [18]. However, under OMVPE growth conditions, H covers the surface from decomposition of the P precursor. The H coverage converts the surface into a (2×2) reconstruction as observed by STM [19], where one H is attached to each surface dimer [19] in order to satisfy the ECR (in the absence of doping elements). We expect that our results and physical interpretations are generally applicable to other surface reconstructions of III/V films terminated with group-V dimers with H.

To obtain the film doping energy during epitaxial growth, we replace one Ga atom in the first (Fig. 4.2) or second (Fig. 4.3) cation layer with a *p*-type dopant atom, and calculate the energy difference between the doped system and the undoped system. The effect of surfactant Sb on doping energy was calculated by replacing surface P dimers with Sb dimers, assuming the surface reconstruction remains the same [20]. The effect of H as the second surfactant was studied by introducing different concentrations and configurations of H on the surface. The film doping energy is defined as:

$$\Delta E_{\text{doping}} = E_{doped} - E_{undoped} + \mu_{\text{Ga}} - \mu_{\text{Dopant}} \quad , (4.1)$$

where E_{doped} ($E_{undoped}$) is the total energy of the doped (undoped) system, i.e., supercell; μ_{Ga} (μ_{Dopant}) is the chemical potential of Ga (Dopant). In general, μ_{Ga} may vary from μ_{Ga} [bulk] + ΔH_f [GaP] (the P-rich condition) to μ_{Ga} [bulk] (the Ga-rich condition) [21], where ΔH_f [GaP] is the GaP enthalpy of formation. Also, μ_{Dopant} is equal to μ_{Dopant} [bulk]. A more accurate chemical potential of Ga can be estimated in the following way.

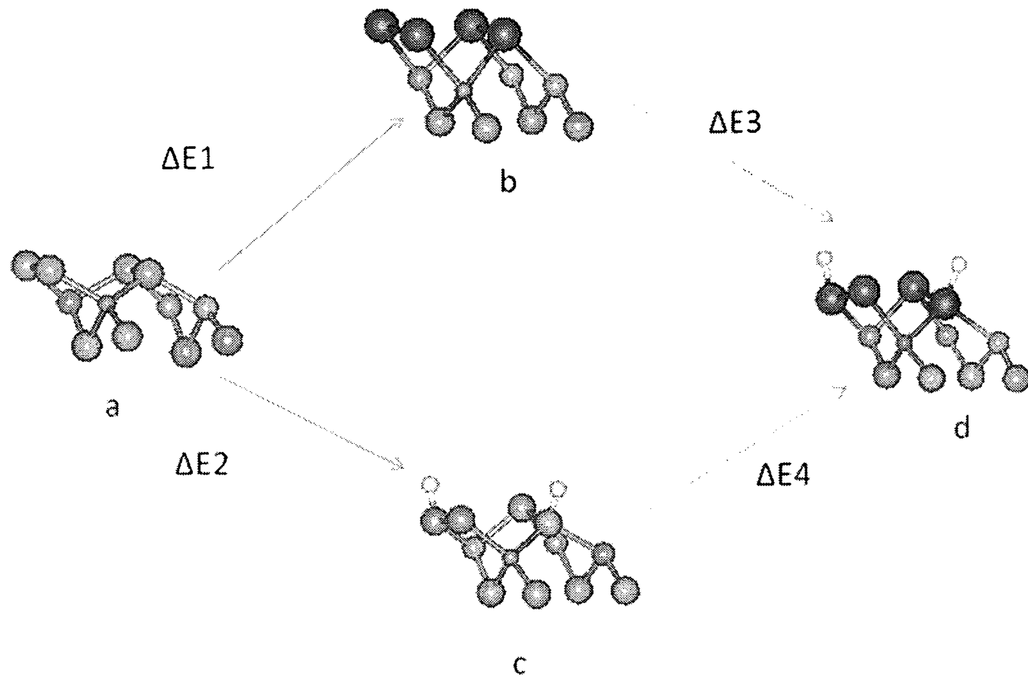

FIG. 4.2. Schematic illustration of various doping configurations, with one P-type dopant atom replacing a Ga atom in the second atomic layer. ΔE indicates the change of doping energy from one configuration to another indicated by the arrows. Largest sphere: Sb; Large sphere: P; medium sphere: Ga; small sphere: p-type dopant; smallest sphere: H.

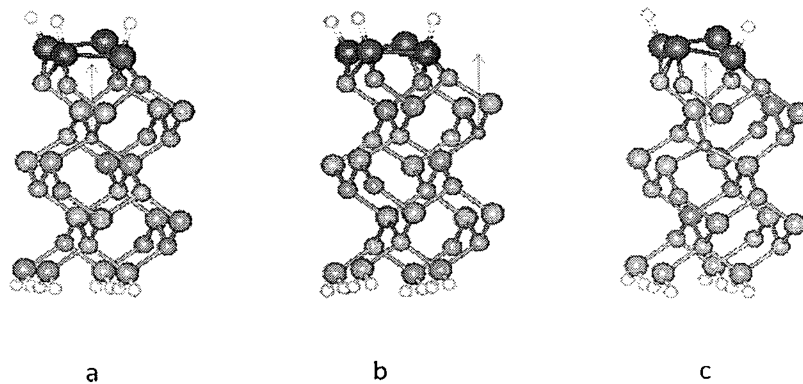

FIG. 4.3. Ball-and-stick schematic illustration of one p type dopant atom doped in the fourth atomic layer (the second cation layer). Atom labels are the same as in Fig. 4.2. (a) dopant atom doped at the site in between two surface dimers with 3 surface H. (b) dopant atom doped at the site below a surface dimer with 3 surface H. (c) dopant atom doped at the site below a surface dimer with 2 surface H and 1 bulk H next to dopant. (The arrows indicate the position of the Zn atom relative to the surface dimer.)

Consider the following reaction at equilibrium: $Ga(l)+1/2P_2(g) \Leftrightarrow GaP(s)$, with ΔG=-158.479 kJ/mol[22] at T =900K, p= 1 atm, the typical growth condition in the OMVPE growth chamber. This gives the partial pressure of P_2 as $P_{P_2} = e^{2\Delta G/RT} = 1.63\times 10^{-7}\,atm$. The actual partial pressure of P_2 in the chamber is much higher, because there is a large amount of P_2 decomposed from PH_3 (the precursor of P_2) through the reaction of $1/2P_2(g)+2/3H_2 \Leftrightarrow PH_3$ at T= 900K and p=1 atm[23]. Therefore, there is no liquid phase Ga. Next, consider $Ga(g)+1/2P_2(g) \Leftrightarrow GaP(s)$, and $\mu_{Ga}+1/2\mu_{P_2}{}^{0} = \mu_{GaP} = \mu_{GaP}{}^{0}$. At 900 K and P_{P2} =1 atm, $\mu_{GaP}{}^{0} = -1.713eV$ and $\mu_{P_2}{}^{0} = -0.685eV$, so $\mu_{Ga} = -1.371eV$. At a different partial pressure of P_2, $\mu_{Ga} = -1.371\,eV + kT\ln P_{P_2}$. However, we are only interested in the change of energy between different surface configurations, so the chemical potential of Ga is cancelled out and not used in our calculations. In the case of H, the film doping energy depends on the chemical potential of H (μ_H) if one additional H is added to the system upon doping. The chemical potential of H is a variable strongly depending upon the growth condition. Here, we choose the typical value of μ_H= -0.67 eV, one-half of the energy of an H_2 molecule at T=900K, p= 1 atm [22]. The value we used in the original analysis [1] would correspond to a H partial pressure of $\sim 10^{-10}$ atm, unrealistically too low at the OMVPE growth conditions. We further note that in the OMVPE growth, there is a large catalytic effect of the phosphide surface on the De-composition of precursors [23]. Therefore, the actual chemical potential of the atomic H may be difficult to estimate due to nonequilibrium conditions at the surface. The chemical potential given here in the gas phase may be considered as the lower limit, because the actual H chemical potential could be higher due to the surface adsorption and decomposition of the precursor [23]. This would lead to a larger doping energy drop due to the extra H than our estimation.

First, we studied the doping energy differences of bulk vs. film without surfactant

effect. We calculated the p-type dopant doping energy in bulk GaP as a reference. Then, we calculated the p-type doping energy in the surface positions of a GaP (001) film, by replacing the Ga in the first cation layer (Fig. 4.2a). Also, to exclude the possible surfactant enhancement effect of H, we do not include H on the top of the (2x2) surface in this calculation. We obtained the bulk and film doping energies for Zn, Be, Mg and Cd shown in Table 4.1. The fourth column of Table 4.1 shows the film doping energy difference for all the dopants with the bulk doping energy as a reference. We found the presence of the surface lowers the doping energy from 0.2 eV to about 1 eV in reference to bulk for different dopants. This difference is possibly due to the covalent radius difference. The covalent radius of Zn is very close to that of Ga and the covalent radius of Be is slightly smaller than that of Ga. Thus, when Zn or Be is incorporated, the difference of doping energy in the bulk vs. in the film is small because of the small strain effect. In contrast, the covalent radius of Cd and Mg are larger than that of Ga, so the presence of surface in the film allows more strain relaxation to accommodate the large size of Cd and Mg and, hence, to reduce the film doping energy much more relative to that in the bulk.

Next, we investigated the surfactant effect of Sb. When Sb is introduced during OMVPE growth, it stays on top of the surface replacing the P surface dimers, due to its large atomic size and lower dangling bond energy (see Fig. 4.2b). This has been demonstrated experimentally by surface photo reflection spectra [24] and is supported by first-principles calculations [20]. To exclude the possible surfactant enhancement effect of H, we at first did not include H on the surface. In our previous study of Zn doping, we replaced surface P dimers with Sb dimers without H (Fig. 4.2b) and obtained $\Delta E_{\mathrm{2nd}}^{\mathrm{Sb,Zn}} = 2.53\,\mathrm{eV} + \mu_{\mathrm{Ga}} - \mu_{\mathrm{Zn}}$, which is 0.07 eV higher than the P dimer case [13]. This

Table 4.1 Doping energies of bulk and film without surfactant for different dopants.

	Bulk	Film	E_{film}-E_{bulk}
Be	$0.23\,\text{eV} + \mu_{Ga} - \mu_{Be}$	$0.02\,\text{eV} + \mu_{Ga} - \mu_{Be}$	-0.21 eV
Zn	$2.69\,\text{eV} + \mu_{Ga} - \mu_{Zn}$	$2.46\,\text{eV} + \mu_{Ga} - \mu_{Zn}$	-0.23 eV
Mg	$2.61\,\text{eV} + \mu_{Ga} - \mu_{Mg}$	$2.14\,\text{eV} + \mu_{Ga} - \mu_{Mg}$	-0.47 eV
Cd	$3.69\,\text{eV} + \mu_{Ga} - \mu_{Cd}$	$2.74\,\text{eV} + \mu_{Ga} - \mu_{Cd}$	-0.95 eV

film doping energy difference is defined as ΔE_1 in Table 4.2.

Here, we performed the same calculation for dopants Be, Mg and Cd, and obtained $\Delta E_{1st}^{Sb,Be} = 0.48\,\text{eV} + \mu_{Ga} - \mu_{Be}$, $\Delta E_{1st}^{Sb,Mg} = 1.99\,\text{eV} + \mu_{Ga} - \mu_{Mg}$ and $\Delta E_{1st}^{Sb,Cd} = 2.93\,\text{eV} + \mu_{Ga} - \mu_{Cd}$, respectively. In comparison to the case of P surface dimers, the corresponding film doping energy changes are $\Delta E_1(Be) = 0.46\,eV$, $\Delta E_1(Mg) = -0.15\,eV$ and $\Delta E_1(Cd) = 0.19\,eV$, as listed in Table 4.2. Importantly, we found that for all p-type dopants studied, the doping energy difference, ΔE_1 (Fig 4.2a vs. Fig 4.2b), between the P dimmer case and Sb dimer case is nearly zero (Zn, Mg) or positive (Cd, Mg). This indicates that Sb alone does not significantly enhance the p-type doping of GaP without H.

Next, we studied the role of H in the doping process. In OMVPE growth, atomic H is produced on the surface [23]. A significant concentration of H (presumably in the form of Zn-H and C-H complexes) is observed in the GaP epitaxial films [8]. Surface H allows the surface to satisfy the ECR [15]. The clean GaP(001)- (2 x 2) model surfaces discussed above do not satisfy the ECR. This provides a thermodynamic driving force for H to incorporate into the film.

In order for the GaP(001)- (2x2) surface to satisfy the ECR, one H can be added to each surface dimer on alternating sides, causing dimer buckling. This has been shown by our calculations to have the lowest energy [13]. When Sb is incorporated as a surfactant, the H bonds to the Sb dimers in the same way (see Fig 4.2d), because Sb is isoelectronic with P. Thus, to investigate the role of H, we calculated the film doping energy with surface H. First, we tested the situation with 2 surface H/cell without Sb (Fig. 4.2c). Assuming that the H coverage remained the same, with two H atoms before and after dopant incorporation. Previously, for Zn doping, we found $\Delta E_{1st}^{P\text{-}2H\to 2H} = 2.68\text{eV} + \mu_{Ga} - \mu_{Zn}$,

Table 4.2. Doping energy difference for p-type dopants.

	Zn	Mg	Cd	Be
ΔE1(eV)	0.07	-0.15	0.19	0.36
ΔE2(eV)	0.22	0.07	0.55	0.41
ΔE3(eV)	-0.78	-0.47	-0.49	-0.92
ΔE4(eV)	-0.93	-0.69	-0.85	-0.97

which is 0.22 eV higher than the case without H, as shown in Fig. 4.2c vs. Fig. 4.2a. This shows that without Sb, H alone does not enhance the doping. This film doping energy difference is defined as ΔE_2 in Table 4.2. We believe that this is largely because the ECR is satisfied before doping, but violated after doping. Here, for the other p type dopants studied, we found a similar trend. The film doping energies for the case with H for Mg, Cd and Be are respectively 0.07, 0.55 and 0.41 eV higher than the case without H, listed as ΔE_2 in Table 4.2. Therefore, we concluded that when H is introduced into the system without Sb, the film doping energy for the *p*-type dopants does not drop.

Next, we investigated the combined effects of Sb and H. Assuming again a surface covered with 2 H/cell before and after the *p*-type dopant incorporation (see Fig. 4.2d), we previously found that for the case of Zn, $\Delta E_{\mathrm{1st}}^{\mathrm{Sb\text{-}2H \rightarrow 2H}} = 1.75\,\mathrm{eV} + \mu_{\mathrm{Ga}} - \mu_{\mathrm{Zn}}$ [13]. Clearly, the Zn film doping energy is substantially reduced, by 0.78 eV, relative to the bare Sb-terminated surface without H from Fig. 4.2b to Fig. 4.2d (defined as ΔE_3 in Table 4.2) and by 0.93 eV relative to the H-covered P-terminated surface without Sb from Fig. 4.2c to Fig. 4.2d (defined as ΔE_4 in Table 4.2). We have termed this intriguing observation as the "dual-surfactant" effect of Sb and H: the two work together in a constructive manner to lower the Zn doping energy, while they do not lower the Zn doping energy individually. For other p-type dopants, we again found a similar trend. As shown by the values of ΔE_3 and ΔE_4 in Table 4.2, the doping energy for Mg with both Sb and H is 0.47 eV lower than the case with only Sb and 0.69 eV lower than the case with only H. The doping energy for Cd with both Sb and H is 0.49 eV lower than the case with only Sb, and 0.85 eV lower than case with only H. The doping energy for Be with both Sb

and H is 0.92 eV lower than the case with only Sb and 0.97 eV lower than the case with only H. Therefore, the dual surfactant effect can be extended to all the p-type dopants studied: *the surfactant Sb and Surface H work together in a constructive manner to lower the p-type doping energy, for a wide range of acceptor element residing on the group III sublattice.*

Next, we investigated the surface configuration with 3 surface hydrogen atoms per 4 Sb atoms. The ECR is violated after the dopant is incorporated if the surface H remains constant. In order to satisfy the ECR, one additional H has to be added. In our previous study of Zn, to quantify the role of the extra H, we calculated the Zn film doping energy by assuming a surface covered with 2 H before, but with 3 H after doping (see Fig. 4.4b to 4c below). We found that $\Delta E_{\rm 1st\,Zn}^{\rm Sb\text{-}2H\to 3H} = -0.63\,{\rm eV} + \mu_{\rm Ga} - \mu_{\rm Zn} - \mu_{\rm H} = 0.04\,{\rm eV} + \mu_{\rm Ga} - \mu_{\rm Zn}$ [13]. Clearly, by adding an extra H after doping to satisfy the ECR, the doping energy of Zn can be decreased further depending on the H chemical potential (μ_H). Here, we examine the similar effect of the third H for the case of Mg/Cd/Be, and find that $\Delta E_{\rm 1st\,Mg}^{\rm Sb\text{-}2H\to 3H} = -0.91\,{\rm eV} + \mu_{\rm Ga} - \mu_{\rm Mg} - \mu_{\rm H} = -0.24\,{\rm eV} + \mu_{\rm Ga} - \mu_{\rm Mg}$, $\Delta E_{\rm 1st\,Cd}^{\rm Sb\text{-}2H\to 3H} = 0.84\,{\rm eV} + \mu_{\rm Ga} - \mu_{\rm Cd}$, and $\Delta E_{\rm 1st\,Be}^{\rm Sb\text{-}2H\to 3H} = -2.38\,{\rm eV} + \mu_{\rm Ga} - \mu_{\rm Be}$ respectively. So once again, the film doping energy of Mg/Cd/Be can be further decreased depending on the chemical potential of H. Since the chemical potential of H we use here is the lower limit, in the actual growth, we expect a larger doping energy drop.

So far, we have shown the dual-surfactant effect of Sb and H in enhancing the p-type doping in the first cation layer, i.e., the surface position. It is also important to investigate the configuration where the dopant replaces a Ga atom at the second cation layer, i.e., the subsurface or "bulk" position. In our previous study of Zn, we considered two possible configurations: one with Zn in the fourth atomic layer between two surface Sb dimers (Fig. 4.3a) and the other directly below the surface Sb dimer (Fig. 4.3b). The

respective doping energies were $\Delta E^{\mathrm{Sb-2H\to 3H}}_{\mathrm{2ndZn,\ between}} = 0.13\mathrm{eV} + \mu_{\mathrm{Ga}} - \mu_{\mathrm{Zn}}$ and $\Delta E^{\mathrm{Sb-2H\to 3H}}_{\mathrm{2ndZn,below}} = 0.21\mathrm{eV} + \mu_{\mathrm{Ga}} - \mu_{\mathrm{Zn}}$ [13]. The 0.08 eV difference between the two reflects the dependence of Zn doping energy on the "atomic-level" stress at these sites [25] and Zn is slightly favored at the tensile sites between surface dimers relative to the compressive sites directly below surface dimers. Here, we have expanded this treatment to include Mg/Cd/Be and found a similar result. The respective doping energies are:
$\Delta E^{\mathrm{Sb-2H\to 3H}}_{\mathrm{2nd,\ Mg\ between}} = 0.3\mathrm{eV} + \mu_{\mathrm{Ga}} - \mu_{\mathrm{Mg}}$ and $\Delta E^{\mathrm{Sb-2H\to 3H}}_{\mathrm{2nd,\ Mg\ below}} = 0.58\mathrm{eV} + \mu_{\mathrm{Ga}} - \mu_{\mathrm{Mg}}$;
$\Delta E^{\mathrm{Sb-2H\to 3H}}_{\mathrm{2nd,\ Cd\ between}} = 1.1\mathrm{eV} + \mu_{\mathrm{Ga}} - \mu_{\mathrm{Cd}}$ $\Delta E^{\mathrm{Sb-2H\to 3H}}_{\mathrm{2nd,\ Cd\ below}} = 1.46\mathrm{eV} + \mu_{\mathrm{Ga}} - \mu_{\mathrm{Cd}}$;
$\Delta E^{\mathrm{Sb-2H\to 3H}}_{\mathrm{2nd,\ Be\ between}} = -2.25\mathrm{eV} + \mu_{\mathrm{Ga}} - \mu_{\mathrm{Be}}$ and $\Delta E^{\mathrm{Sb-2H\to 3H}}_{\mathrm{2nd,\ Be\ below}} = -2.31\mathrm{eV} + \mu_{\mathrm{Ga}} - \mu_{\mathrm{Be}}$. The energy difference between the two sites is 0.28 eV for Mg and 0.36 eV for Cd, which are larger than that of Zn. This is probably due to the larger covalent radius of Mg and Cd[26]. Therefore, the tensile site is even more favored by a larger Mg and Cd. Be is slightly favored at the compressive site, which is due to the smaller covalent radius of Be.

Lastly, we have investigated codoping of the p-type dopant and H into the GaP bulk. Experimental observation indicates that complexes of Zn, P and H form during doping of Zn in GaP [27]. This suggests some H go into the bulk with the acceptor. In our previous Zn study, we have calculated the energies associated with one H incorporation into the bulk with Zn, and determined the Zn-P-H complex structures. Figure 4.3c shows the doping of a Zn atom in the subsurface (or "bulk") position along with an H atom next to it. There will be 2 H atoms remaining on the surface (in comparison to 3 H in Fig. 4.3b), so that the ECR is still satisfied.

When a surface H goes into the subsurface, it changes the dopant bonding configuration, forming a dopant-P-H complex. Without H, the dopant bonds with 4

neighboring P atoms in an *sp*3 hybridization (a tetrahedral structure, Fig. 4.3a). With the extra H, one dopant-P bond is broken to form a P-H bond, and the dopant bonds with 3 neighboring P atoms in an *sp*2 hybridization (a planar structure, Fig. 4.3c). This can also be explained by the ECR. The dopant provides two valance electrons and the H provides one. For both P-H and P-dopant bonds, this takes 3/4 electrons, so their sum gives 3 electrons total to satisfy the ECR. Thus, when H is codoped with dopant, it changes the dopant bonding configuration from *sp*3 to *sp*2 hybridization, forming three dopant-P bonds plus an empty orbital.

The codoping of H with dopant into the bulk is also found to be energetically favorable. The film doping energy at the 2nd-cation-layer positions forming the Zn-P-H complex was found previously $\Delta E_{\text{2nd, Zn}}^{\text{Sb-2H}\rightarrow\text{1 bulk H}} = -0.19\text{eV} + \mu_{\text{Ga}} - \mu_{\text{Zn}}$ [13], which is about 0.2 eV lower than the corresponding cases with all 3 H atoms remaining on the surface. This suggests that there exists a thermodynamic driving force for one H atom to go into the subsurface (or "bulk") with the dopant, i.e., co-doping of the Zn with H. We have further performed the 2nd cation layer Mg/Cd/Be doping calculation. The film doping energy is $\Delta E_{\text{2nd, Mg}}^{\text{Sb-2H}\rightarrow\text{1 bulk H}} = -0.29\text{eV} + \mu_{\text{Ga}} - \mu_{\text{Mg}}$, $\Delta E_{\text{2nd, Cd}}^{\text{Sb-2H}\rightarrow\text{1 bulk H}} = 0.80\text{eV} + \mu_{\text{Ga}} - \mu_{\text{Cd}}$, $\Delta E_{\text{2nd, Be}}^{\text{Sb-2H}\rightarrow\text{1 bulk H}} = -2.59\text{eV} + \mu_{\text{Ga}} - \mu_{\text{Be}}$. All the energies are lower than the corresponding case with all 3H atoms on the surface. Therefore, similar to H codoping with Zn into the bulk, it is confirmed that there is a thermodynamic driving force for one H atom to go into the bulk with Mg/Cd/Be. On the other hand, it is known that H would compensate the *p*-type dopant in bulk GaP, mitigating the doping effect [28,29], which is also confirmed by our electronic structure calculations. To activate the acceptor, annealing can be done after the doping process to remove the H [28,29]. In other words, the codoped H must be removed

after it serves its purpose to assist the dopant incorporation.

Now, based on all the above calculations, we postulate a plausible complete Mg/Cd/Be doping process, the same as the Zn doping process [13] in GaP driven by the dual surfactant effect of Sb and H as shown in Fig. 4.4 for Mg as an example. The doping of Mg in the original P-terminated surface covered with 2 H/cell is shown in Fig. 4.4a. In the first step, with the Sb replacing the P dimers, a Mg atom is doped into the first cation layer (Fig. 4.4b), where it assists the doping process. Two surface H atoms allow the ECR to be satisfied before doping and the Sb plays the role of providing an electron reservoir to accommodate the redistribution of electrons when the ECR is violated after the key step involving exchange of the surface Mg and Ga from the lattice. In the subsequent step, one additional H is added to the surface to further assist the doping process by adding one more electron to satisfy the ECR (Fig. 4.4c). In the third step, the Mg atom goes into the subsurface ("bulk") and replaces a Ga atom in the 2nd or lower cation layers. Simultaneously, a surface H goes together with Mg into the subsurface ("bulk") as a codopant to form a Mg-P-H complex, as shown in Fig. 4.4d, where the ECR is satisfied both at the surface and in the bulk at the complex site. The codoped H needs to be removed later by annealing to activate the acceptor.

The corresponding doping energy changes are shown in Fig. 4.5 for the case of Zn, Mg, Cd and Be. The squares are for Zn. The first step has $\Delta E = -0.93$ eV, showing the energy difference between Sb/2H enhanced system and P/2H system. The second step has $\Delta E = -1.71$ eV, showing the energy difference between the Sb/2H system and Sb/3H system. The third step has $\Delta E = -0.23$ eV, showing the energy difference between Sb/3H and P-Zn-H complex and Sb/3H system. For Mg (circle)/Cd(triangle)/Be(star), the first

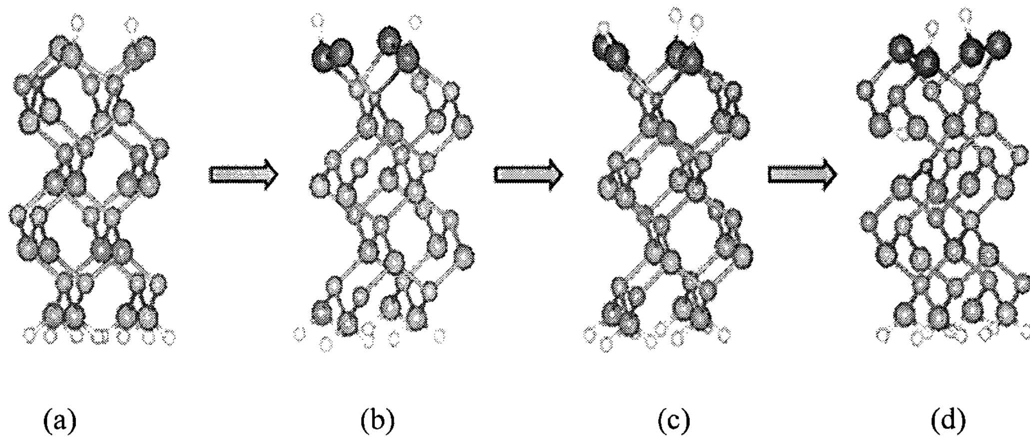

FIG. 4.4. Schematic illustration of a plausible doping process, with one Mg(Zn) atom replacing a Ga atom in GaP film. Atom labels are the same as in Fig. 1. (a) Mg(Zn) doped into the second atomic layer with surface P dimers. (b) Mg(Zn) doped into the second atomic layer replacing Ga with surface Sb dimers. (c) One additional H is added onto the surface to satisfy ECR. (d) H codoped with Mg(Zn) into bulk to form a Mg(Zn)-P-H complex.

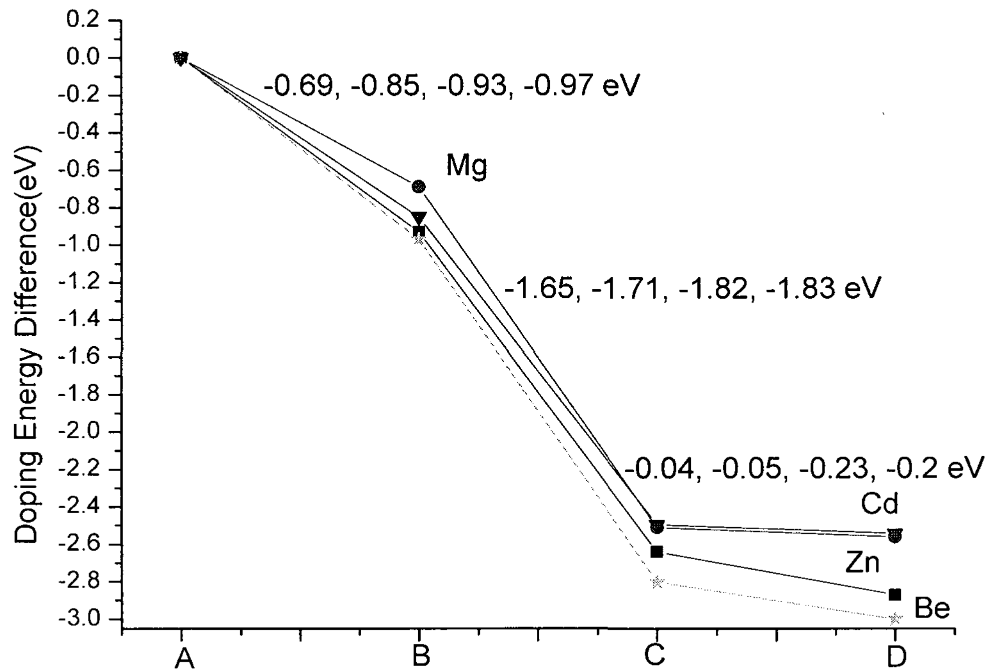

FIG. 4.5. Change of doping energy at each doping step as shown in Fig. 4.4. Square: Zn as doptant; Circle: Mg as dopant. Triangle: Cd; Star: Be.

step has ΔE = -0.69 eV, -0.85 eV and -0.97 eV, respectively, reflecting the role of Sb and 2H as dual surfactants; the second step has ΔE = -1.82 eV, -1.65 eV and -1.83eV, respectively, reflecting the role of the third H (also, in the growth chamber, due to the higher chemical potential of H than our estimated value, the doping energy drop will possibly be greater than the estimation here); the third step has ΔE = -0.05 eV,-0.04 eV and -0.2 eV, respectively, reflecting the energy gain in forming P-Mg/Cd/Be-H complex. Consequently, we have an overall downhill energy landscape for the whole doping process thermodynamically. Notice that the second-step doping energy with one H added to the system depends on the H chemical potential, while the third-step H codoping energy with one H moving from surface to bulk does not. This implies that one may increase the partial pressure of H and, hence, H chemical potential during growth to further enhance p-type doping in the second step. Also, we predict that the dual surfactant effect is the strongest for Be and weakest for Mg and Cd, which still needs further experimental work to prove.

Our theoretical picture of dual-surfactant effect and its underlying physical mechanism based on the ECR is qualitatively consistent with the experimental observation of both the enhanced Zn doping with Sb introduction during OMVPE growth and the co-incorporation of H with Zn [7,8]. However, because the computation is limited to a small cell size, we can only calculate a few representative cases of surface structures, surface coverage and dopant concentrations. Therefore, the actual energy values may vary with these conditions and should be treated with caution. However, the overall trend of the calculated energy changes is expected to be generally correct. Also, other effects, such as temperature and kinetic rates of atom exchange and incorporation, need to be

taken into account in future studies in order to obtain a more complete picture of the dual-surfactant effect. For example, from the energy scales shown in Fig. 4.5, temperature is expected to have a small effect on the film doping energy in step 1 (-0.69,-0.85,-0.93,-0.97 eV for Mg, Cd, Zn and Be, respectively), and a large effect on the H codoping energy in step 3 (-0.04,-0.05, -0.2,-0.23 eV for Cd, Mg, Be and Zn, respectively). However, temperature changes surface H coverage, which will, in turn, affect doping energy. The kinetic barriers associated with each step of the process are also important, but their calculations would go beyond the scope of this work, which focuses on the thermodynamic aspects of doping energies and the underlying physical principles based on ECR. Entropy also enters the free energy calculation. At high temperature limit, the vibrational entropy can be approximated as [30],

$$S = 3R[\ln(T / T_{Debye}) + 4/3] \quad (4.2),$$

where, T_{Debye} is the Debye temperature, which is 445K for GaP[31]. At 900K, the entropy is 50.5 J/Kmol. However, the entropy effect is cancelled out in the calculation of doping energy due to the surfactant effect.

In conclusion, we have discovered an interesting dual-surfactant-codoping effect of Sb and H for p-type doping enhancement for Zn, Cd, Mg and Be. The dual-surfactant with two surface elements will greatly broaden the scope and application of the conventional surfactant effect with one surface element. The two surface H serve as part of the dual surfactant and the H in the bulk serves as a codopant. Specifically, in order to accommodate the *p*-type dopant incorporation, the role of first surfactant Sb (a "metallic" element) is to provide an electron reservoir to redistribute electrons, while the role of two

surfactant H are served to satisfy ECR at surface before the doping, and the codoped H (a "single electron") is to add one electron to satisfy ECR in the bulk after the doping and later by annealing, the codoped H can easily diffuse away. We believe the dual-surfactant effect we disclose here can be used as a general strategy for enhancing *p*-type doping of III-V semiconductors by using a metallic-element with H as dual-surfactants and codopants.

The authors are grateful to DOE-BES for supporting this work. The calculations were performed on AMD Opteron cluster at the CHPC, University of Utah.

4.1 References

[1] M. Copel, M. C. Reuter, E. Kaxiras, and R. M. Tromp. Phys. Rev. Lett. **63**, 632, (1989).

[2] G. Rosenfeld, R. Servaty, C. Teichert, B. Poelsema, and G. Comsa, Phys. Rev. Lett. **71**, 895, (1993).

[3] J. Meyer, J. Vrijmoeth, H. van der Vegt, R. Behm, Phys. Rev. B **51,** 14790, (1995).

[4] M. R. Pillai, Seong-Soo Kim, S. T. Ho, S. A. Barnett, J. Vac. Sci. Technol. B **18**, 1232, (2000).

[5] E. Rudkevich, Feng Liu, D. E. Savage, T. Keuch, L. McCaughan, and M. G. Lagally, Phys. Rev. Lett. **81**, 3467, (1998).

[6] C. M. Fetzer, R. T. Lee, J. K. Shurtleff, G. B. Stringfellow, S. M. Lee and T. Y. Seong, Appl. Phys. Lett. **76**, 1440, (2000).

[7] D. C. Chapman, A. D. Howard, and G. B. Stringfellow, J. Crystal Growth **287**, 647, (2006).

[8] A. D. Howard, D. C. Chapman, and G. B. Stringfellow, J. Appl. Phys. **100**, 44904, (2006).

[9] R. R. Wixom, L. W. Rieth and G. B. Stringfellow, J. Crystal Growth **265**, 367-374, (2004).

[10] W. Shockley, J.L. Moll, Phys. Rev. **119** (5), 1480, (1960).

[11] S.J. Pearton, H. Cho, F. Ren, J.I. Chyi, J. Han, R.G. Wilson, in: R. Feenstra, T.

Myers, M.S. Shur, H. Amano (Eds.), GaN and Related Alloys, vol. 595, Materials Research Society, Warrendale, PA, pp. W10.6.1–W10.6.10, (2000).

[12] J. K. Shurtleff, S. W. Jun and G. B. Stringfellow, Appl. Phys. Lett. **78**, 3038, (2001).

[13] J. Y. Zhu, F. Liu, G. B. Stringfellow, Phys. Rev. Lett. **101**, 196103, (2008)

[14] L. Zhang, E. G. Wang, Q. K. Xue, S. B. Zhang, and Z. Zhang Phys. Rev. Lett. **97**, 126103, (2006).

[15] P. K. Larsen and D. J. Chadi. Phys. Rev. B **37**, 8282, (1988).

[16] S. D. Burnham, G. Namkoong, W. Henderson and W. A. Doolittle, Journ. Of Crystal Growth, **279**, 26-30, (2005).

[17] G. Kresse and J. Hafner, Phys. Rev. B **49**, 14251, (1994); G. Kresse and J. Furthmuller, Comput. Matter **6**, 8245, (1994).

[18] J. A. Appelbaum, G. A. Baraff, and D. R. Hamann Phys. Rev. B **14**, 1623, (1976).

[19] G. Chen, S. F. Cheng, D. J. Tobin, L. Li, K. Raghavachari, and R. F. Hicks, Phys. Rev. B **68**, 121303, (2003).

[20] R. Wixom, N. A. Modine, and G. B. Stringfellow, Phys. Rev. B **67,** 115309, (2003).

[21] Chris G. Van de Walle, and J. Neugebauer, Phys. Rev. Lett. **88**, 066103, (2002).

[22] O. Knacke, O. Kubaschewski K.Hesselmann(Eds.), Thermochemical Properties of Inorganic Substances, Second Edition, Springer-Verlag, pp 728, pp 743, pp 803, (1991).

[23] G. B. Stringfellow, Organometallic Vapor-Phase Epitaxy, Theory and Practice, Second Edition, Academic Press, pp 141, pp 243, (1999).

[24] M. Sugiyama, S. Maeyama, F. Maeda, and M. Oshima, Phys. Rev. B **52**, 2678, (1995).

[25] Feng Liu and M. G. Lagally, Phys. Rev. Lett. **76**, 3156, (1996).

[26] B. Cordero, V. Gómez, A. E. Platero-Prats, M. Revés, J. Echeverría, E. Cremades, F. Barragán and S. Alvarez, Covalent Radii Revisited, Dalton Trans., (2008).

[27] M. D. McCluskey, E. E. Haller, J. W. Walker, and N. M. Johnson, Appl. Phys. Lett. **65**, 2191, (1994).

[28] E. V. K. Rao, B. Theys, Y. Gottesman, and H. Bissesur, 11th International Conference on Indium Phosphide and Related Materials, 0-7803-5562-8/99 IEEE, (1999).

[29] C. H. Chen, S. A. Stockman, M. J. Peanasky, and C. P. Kuo, Semiconductors and Semimetals, Vol 48, ed. by G. B. Stringfellow, M. G. Craford, Academic Press, pp 122-127, (1997).

[30] M. D. Sturge, Statistical and Thermal Physics: Fundamentals and Applications, illustrated edition, A K Peters, Ltd., pp 136, (2003).

[31] M. Ilegems and H. C. Montgomery, Journal. Phys. Chem. Solids, **34**, 885, (1973).

CHAPTER 5

DOPANT INDUCED ELECTRONIC STRESS AND STRAIN ENHANCED DOPING

A common theme of my thesis research work is to make theoretical predictions proposing new methods to enhance p-type doping, or doping in general, of high band gap semiconductors. In addition to the dual-surfactant effect discussed in the last two chapters, I also investigated the possibility of applying external strain as a general strategy to enhance doping of semiconductors. Because the dopant atom usually has a different atomic size (or covalent radius for semiconductors) from the host atom it substitutes, it will induce lattice stress in the host lattice (which is stress free at its equilibrium lattice constant before doping), adding a strain component to the doping energy. Naturally, one expects that by applying external strain, it will be possible to relax the dopant induced stress and, hence, to lower the doping energy. The most significant scientific finding in this part of my study is the discovery of the dopant induced "electronic stress" due to the difference in electronic structure between the dopant and host atom. In other words, even if the dopant has the same atomic size (covalent radius) as the host atom, it will still induce a lattice stress of electronic origin. In general, an n-type dopant, with one extra electron than the host atom, induces a compressive (negative) stress; a p-type dopant, with one less electron than the host atom, induces a tensile (positive) stress. This interesting "electronic stress" effect not only makes a major advancement over the concept of stress in classical elastic theory, but also has significant implications in

applying strain to enhancing doping of semiconductors. In this chapter, I will show extensive DFT calculations to reveal the dopant induced "electronic stress" and its effect on strain enhanced doping. Also, a research paper is to be submitted soon.

5.1 The dopant induced electronic stress in semiconductors

When a dopant atom enters the semiconductor lattice replacing a host atom, it will inevitably induce a lattice stress. Here, we argue that in addition to the conventional stress due to the difference in atomic size between the dopant and host atom [1], there exists another stress component due to the difference in their electronic structure that the dopant atom has either one more or one less valence electron than the host atom for a n-type or p-type dopant, respectively. This novel concept of electronic stress is illustrated in Fig. 5.1. Figure 5.1a shows a two-dimensional stress-free host lattice. Figure 5.1b shows a dopant-induced stress due to the atomic size effect, which we refer to it later as the atomic stress. Figure 5.1c shows a dopant induced stress due to the electronic effect, which we refer to as the electronic stress. It shows the case for an n-type dopant, which adds one more electron in the lattice. Assuming the dopant atom has the same covalent radius (as shown in Fig. 5.1c), it still induces a compressive lattice stress because the extra electron (forming an electron cloud around the dopant indicated by dark area in Fig. 5.1c) applies effectively an internal pressure tending to expand the lattice. Similarly, a p-type dopant also induces an electronic lattice stress, usually a tensile stress, because it removes one electron from the lattice making the lattice tend to contract.

This electronic stress is an interesting new concept, adding an important quantum mechanical aspect to our conventional view of stress based on classical mechanics, which captures only the size effect. We have performed first-principles DFT lattice stress

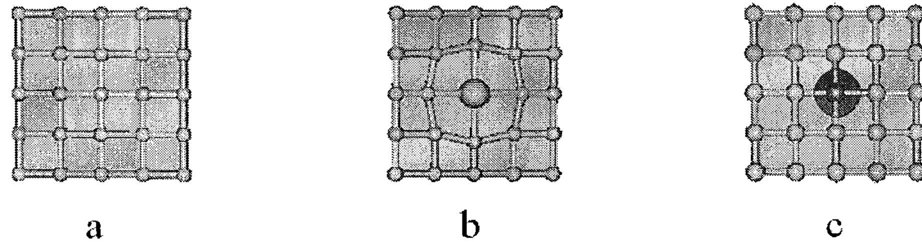

Fig. 5.1. Schematic illustration of a dopant induced stress applied to a 2D lattice. (a) undoped strain free lattice; (b) a compressive stress induced by a large dopant; (c) a compressive stress induced by an n-type dopant.

calculations to reveal such electronic stress effect, using the VASP code [2] within the local density approximation. We choose GaP as our model system. Our simulation cell is a 4x4x4 cell consisting of 32 GaP units. We used a plane wave cutoff energy of 340 eV and a 4×4×4 k-point mesh for Brillouin zone sampling. Total energy minimization was performed by relaxing atomic positions until the forces converged to less than ~ 0.1 meV/Å. We tested our idea on various types of dopants including Zn, Al, Cd, In, Si, Ge, and Be and calculated the stress they induce in the GaP lattice. The results are listed in Table 5.1.

The most revealing case is Zn. It is well known that the covalent radius of Zn (1.22±0.04 Å) is almost the same as that of Ga (1.22±0.03 Å) [3]. So, when Zn is doped into GaP replacing Ga, one would expect that it will induce little lattice stress considering only the atomic size effect. On the contrary, however, our DFT calculations showed clearly that it induces a large local tensile stress of 45.95 meV/ $Å^3$ per dopant (Here the lattice stress is divided by the atomic volume to achieve the local stress, which is unchanged with the change of the cell size), or a lattice stress of 0.718 meV/$Å^3$ in a 64-atom lattice (Note that, $\sigma = \frac{1}{3}(\sigma_{xx} + \sigma_{yy} + \sigma_{zz})$.). Since there is no atomic stress contribution, we regard the Zn induced stress as purely electronic stress. The positive sign means the stress is tensile for a p-type dopant. To further confirm this point, we performed a calculation of replacing Ga by Al for comparison. Aluminum, isoelectronic with Ga, is not a dopant, so there will be no electronic stress effect; also, it has about the same covalent radius (1.21±0.04 Å) as Ga, so there will almost be no atomic stress effect either. Indeed, our calculations showed that Al induces a small compressive local stress of -23.17 meV/ $Å^3$ per dopant, or a lattice stress of -0.362 meV/$Å^3$ in GaP, consistent

Table 5.1, Dopant induced stress in an unstrained host lattice of GaP, the covalent radius values are adapted from Reference [3].

Dopant	Local (Lattice) Stress (meV/Å^3))	Dopant Type	Covalent Radius(Å)
Zn	45.95 (0.718)	p	1.22±0.04
Al	-23.17(-0.362)	neutral	1.21±0.04
Cd	-227.2(-3.55)	p	1.44±0.09
In	-275.2(-4.30)	neutral	1.42±0.05
Ge	-19.2(-0.300)	n	1.20±0.04
Si	138.9(2.17)	n	1.11±0.02
Be	324.5(5.07)	p	0.96±0.03

with the fact that the lattice constants of AlP (5.46 Å) [4] are slightly larger than that of GaP (5.45 Å) [5] at standard state.

Zinc is a special case of dopant in GaP, as it induces mostly only the electronic stress. Most dopants have a different atomic size from the host atom, so they will induce both local stress and electronic stress. As an example, we studied the case of Cd, also a p-type dopant like Zn, but its covalent radius is 1.44±0.09 Å much larger than that of Ga (1.22 ±0.04 Å) [3]. Overall, we found that Cd induces a local compressive stress of -227.2 meV/ $Å^3$, or a lattice stress of -3.55 meV/$Å^3$ in a 64-atom GaP lattice, as listed in Table 5.1, which has both atomic and electronic stress contributions. For comparison, we calculated the stress induced by In replacing Ga. Indium, isoelectronic with Ga, is not a dopant, so there will be no electronic stress effect; however, its atomic size (covalence radius of 1.42±0.05 Å) is much larger than that of Ga, so it induces a larger compressive local stress of -275.2 meV/Atom, or a lattice stress of -4.30 meV/$Å^3$, as listed in Table 5.1. However, if we compare the stress induced by Cd versus In, we see that despite the fact that the atomic size of Cd (1.44±0.09Å) is slightly larger than In (1.42±0.05 Å), the Cd induces a noticeably smaller compressive (negative) stress than In. If there were only the atomic size induced stress, the compressive stress induced by Cd would be slightly larger than that induced by In. The difference must be due to the electronic stress induced by Cd as a p-type dopant. Specifically, the electronic stress induced by Cd must have contributed a tensile (positive) stress component that compensates the compressive (negative) stress induced by its atomic size effect, making the overall compressive stress smaller. So, once again, these calculated results show that the p-type dopant induces a tensile stress in the host lattice.

Since the p-type dopant induces a tensile stress, conversely, we expect the n-type dopant to induce a compressive stress. One way to view this is that the n-type dopant adds one extra electron in the lattice that tends to expand the lattice. This physical observation is indeed confirmed by our DFT calculations. We have chosen Ge and Si to replace Ga as n-type dopants in GaP. (We note that if they replace P in GaP, they would act as p-type dopants. The real situation can be more complicated [6]; here we just use them as n-type dopants for model calculations.) The covalent radius of Ge is 1.20±0.04 Å, which is slightly smaller than the covalent radius of Ga (1.22±0.03 Å) [3]. Therefore, if there were only atomic size effect, Ge would induce a small tensile stress in GaP. On the contrary, however, we actually found Ge induces a small compressive local stress of -19.2 meV/Å^3, or a lattice stress of -0.30 meV/Å^3, as listed in Table 5.1. This indicates that as an n-type dopant, Ge induces a compressive electronic stress that overcompensates the tensile atomic stress making the overall stress slightly compressive. For the case of Si, its atomic size (1.11±0.02 Å) is much smaller than that of 1.22 Å. So, it induces a large tensile atomic stress, whose magnitude is large than that of the compressive electronic stress it induces as a n-type dopant. As a result, the overall stress is found to be tensile (a local stress of 138.9 meV/Å^3, or a lattice stress of 2.17 meV/Å^3), as listed in Table 5.1. Despite the discussions above, the exact physical origin of the dopant induced electronic stress is still unclear.

The largest lattice stress a dopant can induce is when its induced atomic stress works in the same direction as its electronic stress without compensating effects, namely a n-type dopant with a larger atomic size than the host atom, both contributing a compressive stress, or a p-type dopant with a smaller atomic size than the host atom, both

contributing a tensile stress. We have identified one such example in Be as a p-type dopant that has a covalent radius (of 0.96 Å) much smaller than Ga. Indeed, we found Be induces the largest tensile local stress of 324.5 meV/Å^3, or a lattice stress of 5.07 meV/Å^3, in GaP as listed in Table 5.1, amongst all the cases we have studied.

5.2 The effect of strain on doping energy

Given the dopant induced lattice stress, naturally one can think of applying an external strain to relax the stress and, hence, to lower the doping energy. The idea of using strain to enhance doping has drawn interest in semiconductor industry before, especially in the metal-oxide-semiconductor devices based on Si systems. In 2002, Sadigh et al. suggested that biaxial strain should have a large effect on the solubility of dopant atoms in Si [7]. Based on their calculation, they suggested that the solubility of B can be enhanced by a compressive strain due to the small size of B. Later, Addey et al. predicted an enhancement of the concentration of As by a tensile strain in Si and explained the effect in terms of a strain induced change in the Fermi Energy [8]. Very recently, Ahn et al. proposed a general theory of strain effects on the solid solubility of impurities impurities suggesting that the strain compensation energy resulting from the strain induced change of the Fermi energy is the primary contribution to the solubility enhancement [1]. All the work to date has focused on Si. However, there is no experimental observation of the strain enhanced doping in Si yet, except that the strain reduced activation barrier for Sb in Si was observed [9,10]. Here, we will extend the idea of strain enhanced doping to III-V semiconductors. Most importantly, we will include the effect of electronic stress in effect of electronic stress in addition to the atomic stress that has been only considered before, and then base our stress and strain energy analysis on elastic theory coupled with first-principles DFT calculations.

We have calculated the doping energy as a function of strain for all the dopants listed in Table 5.1. The doping energy is defined as E(doping) = E(doped) – E(reference)+μ(Ga) – μ(dopant), where E(doped) is the total energy of the doped system, E(reference) is the total energy of the undoped system, μ(Ga) and μ(dopant) are the chemical potential of the Ga and dopants. Since we are primarily interested in the change of doping energy due to strain, the two chemical potential terms will be cancelled out by setting the doping energy of the unstrained system as the zero point of energy. We here considered two different forms of strain: hydrostatic strain and biaxial strain. In applying hydrostatic strain, we change all three cell dimensions of the cubic supercell along x, y, and z equally; in applying biaxial strain, we change the two supercell dimensions along x and y equally and allow the cell dimension along z axis to relax until the energy is minimized.

Considering first hydrostatic strain, Fig. 5.2 shows the calculation results of doping energy (E_d) as a function of hydrostatic strain (ε) for Zn, Cd, Ge, Si and Be. In general, the strain-dependent doping energy can be understood following simple elastic theory as

$$E_d = \int_V \sigma_{di}(\varepsilon) d\varepsilon \,, \qquad (5.1)$$

where σ_{di} is the dopant induced stress in the unstrained lattice. The sign determines how strain will affect doping energy. If a dopant, such as Zn, Si and Be, induces a tensile stress (positive σ_{di}), as shown in Table 5.1, then the curve in Fig. 5.2 has a positive slope and applying negative (compressive) strain will lower the doping energy. If a dopant induces a compressive stress (negative σ_{di}), such as In and Ge as shown in Table 5.1, then the curve in Fig. 5.2 has a negative slope and applying positive (tensile) strain will lower

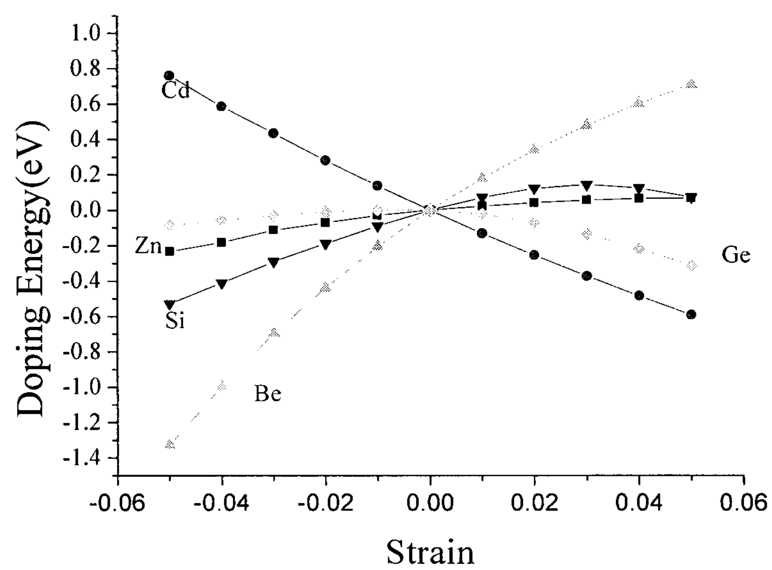

Fig. 5.2. Doping energy vs. hydrostatic strain for the dopants studied.

the doping energy.

Of course, larger values of σ_{di} give a stronger strain effect. In Fig. 5.2, we see that strain has the largest effect on Be whose doping energy can be reduced by as much as 0.2 eV with the application of 1% compressive hydrostatic strain. Therefore, the strain enhanced doping effect in GaP is largest for Be among all the p-type dopants.

The nature of the dopant induced lattice stress, especially the different electronic stress induced by a n-type dopant versus a p-type dopant in addition to their common atomic size effect will help us to better understand how to apply external strain as a possible means to enhance doping in semiconductors. Taking the example of Zn, without electronic stress one would expect that strain has a minimal effect on the Zn doping energy in GaP because its atomic size is about the same as the Ga. However, we can clearly observe in Fig. 5.2 that compressive strain noticeably enhances Zn doping in GaP because it induces a sizable tensile electronic stress (see Table 5.1) as a p-type dopant. Cd is much larger than Ga, so it induces a large compressive atomic stress in GaP, but as a p-type dopant, it also induces a tensile electronic stress that compensates the atomic stress. As a result, the effect of strain on the Cd doping energy is much smaller than what would be expected based on its atomic size effect alone.

The competition between the atomic and electronic stresses is also manifested in the n-type dopants, Si and Ge. The covalent radii of both Si and Ge are smaller than that of Ga, which induces a compressive atomic stress. On the other hand, both are n-type dopants, which induces a tensile electronic stress. Their competition makes the overall net local stress to be positive (tensile) of 138.9 meV/Å^3 (or a lattice stress of 2.17 meV/Å^3) for Si but negative (compressive) local stress of -19.2 mev/Å^3 (or a lattice stress

of -0.30 meV/Å^3) for Ge (see Table 5.1). Consequently, when a small strain is applied (nearby the ε=0 point), the doping energy of Si and Ge show the opposite strain-dependent behaviors, with Si having a positive slope for $|\varepsilon| < 3\%$ and Ge having a negative slope for $|\varepsilon| < 1\%$, as shown in Fig. 5.2. However, when a large strain is applied, we found a very interesting phenomenon that the doping energies of both Si and Ge behave in the same manner; they decrease with either increasing compressive or increasing tensile strain. In other words, one can enhance doping of Si or Ge in GaP by applying a sufficiently high external strain whether it is compressive or tensile. This unusual behavior is found to be caused by the highly nonlinear strain dependence of the dopant induced electronic stress, as we explain in detail below.

5.3 The nonlinear strain dependence of electronic stress

We discovered a significant difference between the atomic stress and electronic stress in their strain dependence. The atomic stress arising from the atomic (or lattice) size difference has generally a linear dependence on strain, so it can be readily treated with the linear elastic theory. For example, in Fig. 5.3a, we plotted the DFT calculated atomic lattice stress induced by In and Al (both are nondopants) in GaP as a function of external hydrostatic strain, showing an almost linear behavior. In contrast, in Fig. 5.3b, the lattice stress induced by Zn and Si is highly nonlinear. In particular, we note that the stress induced by Zn is almost completely electronic stress, while the stress induced by Si has both atomic and electronic components. These results clearly indicate that the dopant induced electronic stress in semiconductors has a highly nonlinear dependence on strain. This will in turn give rise to a highly nonlinear strain dependence of doping energy, as shown in Fig. 5.2.

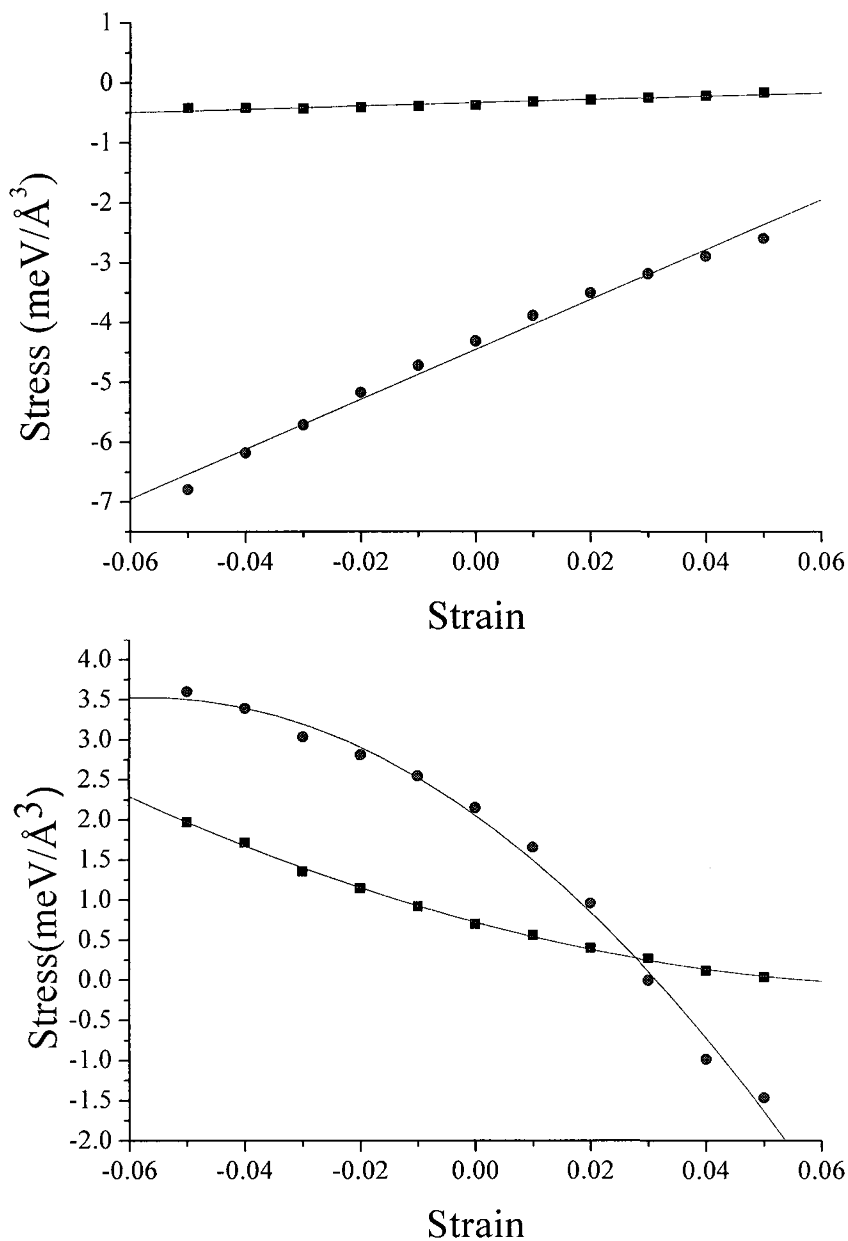

Fig. 5.3. Dopant induced stress vs. hydrostatic strain. (a) Square: Al, dots: In. Solid lines are linear fits to the data. (b) Square: Si, dot: Zn. Solid lines are parabolic fits to the data.

Based on the dopant induced stress-strain relationship, we can calculate the doping energy as a function strain based on elastic theory as shown in Eq. (5.1). Now, we know the function of $\sigma_{di}(\varepsilon)$ from the fitting to the DFT calculations as shown in Fig. 5.3:

$$\sigma_{di}(\varepsilon) = \sigma_{di}(0) + C_1\varepsilon + C_2\varepsilon^2, \qquad (5.2)$$

where $\sigma_{di}(0)$ is the dopant induced stress in the unstrained lattice as listed in Table 5.1. C_1 and C_2 are elastic constants obtained by fitting to the DFT calculated results as shown in Fig. 5.3. The doping energy can be readily calculated by substituting Eq. (5.2) into (5.1), as

$$E_d(\varepsilon) = 3V[\sigma_{di}(0)\varepsilon + (1/2)C_1\varepsilon^2 + (1/3)C_2\varepsilon^3]. \qquad (5.3)$$

The prefactor 3V comes from volume integration of Eq. (5.1). We found that using the data of C_1 and C_2 from the fitting to the dopant-induced stress (Fig. 5.3), Eq. (5.3) gives an excellent fitting to all the strain-dependent doping energies, as shown in Fig. 5.4, for the case of Zn and Si as examples.

Compare the case of Zn and Si in Fig. 5.4, Zn, a p-type dopant, induces a tensile electronic stress, whose effect seems to be more dominant when a compressive external strain is applied to lower its doping energy, while when a tensile strain is applied, the doping energy changes less. Conversely, Si, an n-type dopant, induces a compressive electronic stress, whose effect seems to be more dominant when a tensile external strain is applied. In particular, its electronic stress has to compete with its atomic stress to define the final outcome. When a large enough tensile strain is applied (> 3%), the

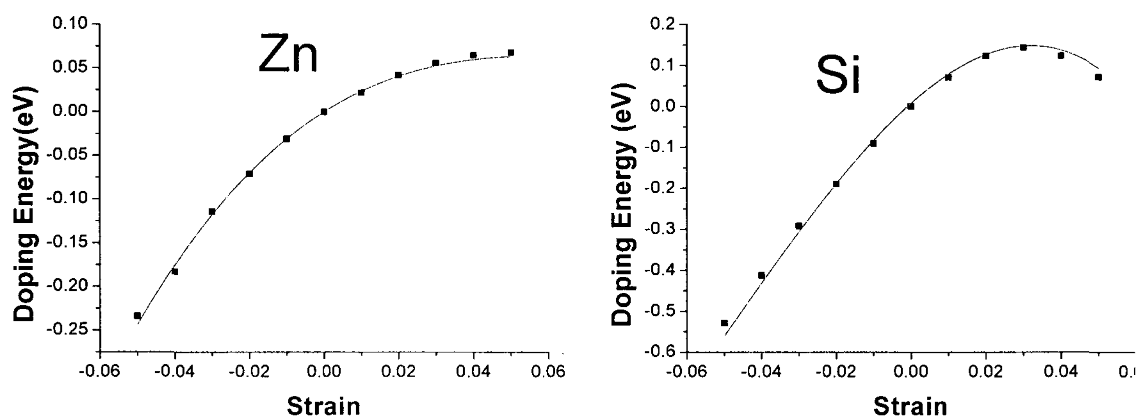

Fig. 5.4. Doping energy of Zn and Si versus hydrostatic strain, showing the excellent fitting of the elastic theory (solid line) to the DFT calculated data (dots).

compressive electronic stress can overcome the tensile atomic stress so that the doping energy decreases with the increasing tensile strain. In contrast, when a compressive strain is applied, the tensile atomic stress is the dominating factor so that the doping energy also decreases with the increasing compressive strain. Therefore, it is the nonlinear strain dependence that gives rise to the unusual strain dependence of doping energy of Si as well as Ge shown in Fig. 5.3.

5.4 Enhanced doping using Epitaxial Strain

Our final goal is to propose possible ways of applying strain to enhancing doping in semiconductors. Hydrostatic strain is difficult to apply. However, biaxial strain is applied in the process of heteroepitaxial growth of thin films when a thin film material of one lattice constant is grown on a substrate of a different lattice constant. Thus, we performed the calculations of doping energy versus biaxial epitaxial strain. Based on the above hydrostatic strain calculations, we chose Be as the dopant because it shows the largest strain enhancement of doping energy due to the fact that both the atomic and electronic stress it induces in GaP are tensile working in the same direction. In applying the biaxial strain, we changed the unit cell along the x and y axes by an equal amount and relaxed the unit cell along the z axis to minimize the energy. For unstrained GaP, we calculated $\varepsilon(z) / \varepsilon(x) = -0.90$, where $\varepsilon(z)$ is the strain along z and $\varepsilon(x)$ is the strain along x. This ratio agrees well with the experiment value $-2C(12) / C(11) = -0.89$ [11]. The results are shown in Fig 5.5, in comparison with the hydrostatic strain calculations. The circles are the doping energies calculated for different biaxial strain. The squares are the doping energies calculated for hydrostatic strain. From Fig. 5.5, we found that the doping energy is enhanced for about 100 meV for a one percent biaxial compressive strain.

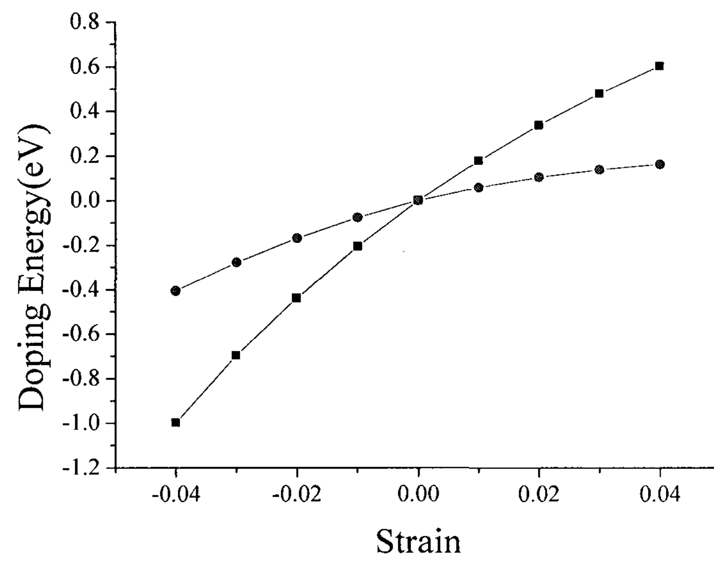

Fig. 5.5, Doping energy vs. biaxial strain and hydrostatic strain for Be in GaP. Circle: biaxial strain; Square: hydrostatic strain.

Therefore, the Be concentration can be enhanced for more than 3 times under a typical OMVPE growth temperature of 900 K for GaP. The trends of strain enhanced doping for the biaxial case and hydrostatic case are about the same, except that the effect of biaxial strain is smaller than that of hydrostatic strain. The doping energy enhancement under compressive strain for the biaxial strain is about 40 % of that for the hydrostatic strain. We can conclude that applying a biaxial strain can effectively enhance the solubility of the Be in GaP.

We have discussed an intriguing dopant-induced electronic stress effect we discovered in this chapter. The dopant-induced stress has generally two components: an atomic size effect and an electronic effect. For the electronic effect, n-type dopants induce a compressive stress due to the extra electron added to the system. This tends to expand the lattice; p-type dopants induce a tensile stress due to the electron deficit that tends to shrink the lattice. We also found that the electronic stress exhibits a nonlinear dependence on strain, different from the conventional atomic stress behavior. The dopant induced total stress in the unstrained lattice determines how the strain affects doping. Our work broadens the scope of conventional stress effect that takes into account only the atomic size effect. We also proposed a strain enhanced doping strategy for III-V semiconductors and predicted that for p-type dopants, Be has the highest strain enhanced doping effect.

5.5 References

[1] C. Ahn, N Bennett, S. T. Dunham, and N. B. Cowernl, Phys. Rev. B **79**, 073201, (2009).

[2] G. Kresse and J. Hafner, Phys. Rev. B **49**, 14251 (1994); G. Kresse and J. Furthmuller, Comput. Matter **6**, 8245, (1994).

[3] B. Cordero, V. Gómez, A. E. Platero-Prats, M. Revés, J. Echeverría, E. Cremades, F. Barragán and S. Alvarez, Covalent Radii Revisited, Dalton Trans., (2008).

[4] O. Madelung, U. Rössler and M. Schulz, Group IV Elements, IV-IV and III-V Compounds. Part b - Electronic, Transport, Optical and Other Properties, Landolt-Börnstein - Group III Condensed Matter, Numerical Data and Functional Relationships in Science and Technology, Springer-Verlag, pp. 3, (2002).

[5] L. I. Berger , Semiconductor materials, Physical Sciences References Series, Illustrated Edition, CRC Press, pp. 134, (1997).

[6] P. J. Dean, C. J. Frosch and C. H. Henry J. appl. Phys. **39,** 563146, (1968).

[7] B. Sadigh, T. J. Lenosky, M. Caturla, A. A. Quong, L. X. Benedict, and T. Diaz de la Rubia, Appl. Phys. Lett. **80**, 4738, (2002).

[8] J. Adey, R. Jones, and P. R. Briddon, Phys. Status Solidi C **2**, 1953, (2005).

[9] N. S. Bennett, N. E. B. Cowern, A. J. Smith, R. M. Gwilliam, B. J. Sealy, L. O'Reilly, P. J. McNally, G. Cooke and H. Kheyrandish, Appl. Phys. Lett. **89**, 182122, (2006).

[10] N. S. Bennett, A. J. Smith, R. M. Gwilliam, R. P. Webb, B. J. Sealy, N. E. B. Cowern, L. O'Reilly and P. J. McNally, J. Vac. Sci. Technol. B **26**, 391, (2008).

[11] Raoul Weil and Warren O. Groves, J. Appl. Phys. **39**, 4049, (1968).

CHAPTER 6

CONCLUSIONS

In this thesis, extensive doping energy calculations of GaP thin films based on DFT have been performed. These calculations led to two important discoveries: one is the dual surfactant effect on enhancing p-type doping in GaP, and the other is the dopant-induced electronic stress effect.

Surfactant effects are usually achieved by the addition of one surface element. In our calculation, we have discovered an intriguing dual-surfactant effect of Sb and H for various *p*-type doping enhancement in GaP, including Zn, Cd, Mg and Be.

We first demonstrated by our calculation that Sb as a surfactant alone can not enhance the doping of Zn (replacing a Ga atom on the first cation layer) for GaP. Also, H alone as a surfactant can not enhance the doping of Zn for GaP as well. The doping energy of Zn in GaP is lowered by about 0.8 eV only when both Sb and H are introduced on the surface of the GaP thin film as dual surfactants. The two surface H atoms, which attach to the surface anion dimers, serve as a part of the dual surfactant effect by providing two electrons that satisfy the ECR before doping. In order to accommodate the *p*-type dopant incorporation, surface Sb atoms have to be incorporated with H. The role of the surfactant Sb (a "metallic" element) is to provide an electron reservoir to redistribute electrons. In the next step, we studied the case of Zn replacing a second

cation layer Ga atom and found the doping energy of Zn is further lowered for the Zn atom going down to the second cation layer and between two surface dimers. Also, to lower the doping energy in the 2nd cation layer (or the "bulk" situation), an additional H atom was introduced in our calculation into the "bulk" to serve as a codopant, which provides one more electron that satisfies the ECR after doping. This extra H can form a planar SP^2 like bonding configuration with P in the bulk. We also proposed a possible doping process based on our calculation and provided the change of doping energy for each step and found that the doping energy of Zn is the lowest when Zn atom replaces a second cation Ga atom at the site between two surface dimers and an extra H is incorporated into the bulk.

We subsequently expanded our calculation to other p-type dopants, Mg, Cd and Be, which replace the cation host atoms. We found a similar dual surfactant effect for all these dopants. Among all of these 4 p-type dopants, the dual surfactant effect is found to be weakest for Mg, because its metallic nature negates the effect of Sb. The highly metallic Mg may also explain why Mg is a successful *p*-type dopant in III-V semiconductors. We believe the dual-surfactant effect we disclose here can be used as a general strategy for enhancing *p*-type doping of III-V semiconductors by using a metallic-element with H as dual-surfactants and codopants. This dual surfactant effect can be generalized as a basic doping enhancement rule: the doping of the metallic p-type dopants can be enhanced only when the ECR is satisfied before doping and the metallic elements replace the surface anion atoms and serve as electron reservoirs.

For the dopant induced electronic stress, our calculations show that even when a dopant has the same atomic size (covalent radius) as the host atom, such as Zn replacing

Ga, it still induces a sizable electronic stress. In general, an n-type dopant, such as Si and Ge, induces a compressive electronic stress; a p-type dopant, such as Zn and Be, induces a tensile electronic stress. The competition between the atomic stress and the electronic stress determines the overall stress induced by a dopant. Sometimes, they work in a different direction and cancel each other, such as small n-type dopant, Si, or a large p-type dopant, Cd. Sometimes, they work in the same direction and induce a large stress, such as a small p-type dopant, Be, or a large n-type dopant. We also proposed a strain enhanced doping strategy for III-V semiconductors and predicted that for p-type dopants, Be has the highest strain enhanced doping effect.

This thesis indicates that DFT calculations are a very useful tool to study OMVPE problems, especially when the *in situ* observation of the surface is difficult or impossible, which is often the case with OMVPE. The dual-surfactant effect will greatly enhance our general understanding of semiconductor doping and broaden the scope and application of the conventional surfactant effect with one surface element. Our work of the dopant induced electronic stress and strain enhanced doping broadens the scope of conventional stress effect that takes into account only the stress induced by the difference in the atomic size. It will be very interesting to have future experiments to try out the proposed mechanism of strain enhanced doping in III-V semiconductors and confirm the existence of electronic stress.